

The Unexpected Protective Role of Thrombosis in Sepsis-Induced Inflammatory Lung Injury Via Endothelial Alox15

Authors: Colin E. Evans^{1, 2, 3}, Xianming Zhang^{1, 2, 3}, Narsa Machireddy^{1, 2, 3}, and You-Yang
Zhao^{1, 2, 3, 4, 5, 6*}

Affiliations: 1. Program for Lung and Vascular Biology; and 2. Section for Injury Repair and Regeneration Research, Stanley Manne Children's Research Institute, Ann & Robert H. Lurie Children's Hospital of Chicago, Chicago, Illinois, USA. 3. Department of Pediatrics, Division of Critical Care, Northwestern University Feinberg School of Medicine, Chicago, Illinois, USA. 4. Department of Pharmacology; 5. Department of Medicine, Division of Pulmonary and Critical Care Medicine; 6. Feinberg Cardiovascular and Renal Research Institute; Northwestern University Feinberg School of Medicine, Chicago, Illinois, USA.

*Correspondence: youyang.zhao@northwestern.edu.

1 **Abstract:**

2 **Background.** Patients with sepsis-induced acute lung injury (ALI)/acute respiratory distress
3 syndrome (ARDS) commonly suffer from severe pulmonary thrombosis, but clinical trials of anti-
4 coagulant therapies in sepsis and ARDS patients have failed. ARDS patients with
5 thrombocytopenia also exhibit increased mortality, and widespread pulmonary thrombosis is often
6 seen in coronavirus disease 2019 (COVID-19) ARDS patients.

7 **Methods.** Employing different amounts of microbeads to induce various levels of pulmonary
8 thrombosis. Acute lung injury was induced by either lipopolysaccharide i.p. or cecal ligation and
9 puncture. Endothelial cell (EC)-targeted nanoparticle coupled with CDH5 promoter was employed
10 to delivery plasmid DNA expressing the CRISPR/Cas9 system for EC-specific gene knockout or
11 expressing *Alox15* for EC-specific overexpression. Additionally, thrombocytopenia was induced
12 by genetic depletion of platelets using *DTR^{Pf4Cre}* mice by breeding *Pf4Cre* mice into the genetic
13 background of *DTR* mice.

14 **Results.** We show that while severe pulmonary thrombosis or thrombocytopenia augments
15 sepsis-induced ALI, the induction of mild pulmonary thrombosis conversely reduces endothelial
16 cell (EC) apoptosis, ALI, and mortality via sustained expression of endothelial arachidonate 15-
17 lipoygenase (*Alox15*). Endothelial *Alox15* knockout via EC-targeted nanoparticle delivery of
18 CRISPR/Cas9 plasmid DNA in adult mice abolished the protective impact of mild lung thrombosis.
19 Conversely, overexpression of endothelial *Alox15* inhibited the increases in ALI caused by severe
20 pulmonary thrombosis. The clinical relevance of the findings was validated by the observation of
21 reduced ALOX15-expressing ECs in lung autopsy samples of ARDS patients. Additionally,
22 restoration of pulmonary thrombosis in thrombocytopenic mice also normalized endotoxemia-
23 induced ALI.

24 **Conclusion.** We have demonstrated that moderate levels of thrombosis protect against sepsis-
25 induced inflammatory lung injury via endothelial Alox15. Overexpression of Alox5 inhibits severe
26 pulmonary thrombosis-induced increase of ALI. Thus, activation of ALOX15 signaling represents
27 a promising therapeutic strategy for treatment of ARDS, especially in sub-populations of patients
28 with thrombocytopenia and/or severe pulmonary thrombosis.

29 **Key Words:** Acute lung injury, acute respiratory distress syndrome, ALOX15, endothelial cells,
30 inflammation, sepsis, thrombosis

31 Introduction

32 Sepsis is an infection-induced uncontrolled inflammatory response that often results in
33 acute lung injury (ALI)/acute respiratory distress syndrome (ARDS) ¹⁻³. Despite improvements in
34 supportive care for patients with ALI/ARDS, including mechanical ventilation and antibiotic
35 therapy, there is currently no effective treatment for ALI/ARDS, and mortality rates for patients
36 with ARDS are as high as 40% ¹⁻³. The lack of effective treatments for ALI/ARDS is likely due to
37 an incomplete understanding of the mechanisms that control the pathogenesis of ALI/ARDS.
38 Given that anti-inflammatory therapies have been unsuccessful in the treatment of ARDS ^{4,5}, it is
39 likely that ALI/ARDS is regulated by factors other than inflammation alone. For instance,
40 ALI/ARDS is characterized by increased levels of thrombosis ^{1, 6, 7}. Widespread pulmonary
41 thrombosis is often seen in coronavirus disease 2019 (COVID-19) ARDS patients ⁸⁻¹¹.
42 Thrombocytopenia is also associated with increased mortality in patients with sepsis and ARDS
43 ¹²⁻¹⁴. Increased microvascular thrombosis and thrombocytopenia are hallmarks of disseminated
44 intravascular coagulation (DIC), which is common in sepsis and ARDS patients ¹⁵⁻¹⁷. However,
45 the impact of thrombosis and thrombocytopenia on ALI is ambiguous ¹⁸. For example, pulmonary
46 thrombosis impedes the delivery of oxygen and nutrients from blood to the lung, while
47 simultaneously acting as a barrier to prevent bacterial exchange ^{19,20}. Crucially, comprehensive
48 investigations of the impact of varying levels of pulmonary thrombosis and of the underlying
49 mechanisms on ALI/ARDS are absent to date.

50 Another characteristic of ALI/ARDS is increased lung endothelial cell (EC) apoptosis and
51 injury ²¹⁻²³. A viable lung EC monolayer is essential for the maintenance of vascular homeostasis
52 ²⁴⁻²⁶, while reduced lung EC survival leads to impaired endothelial barrier function, including
53 increased capillary permeability and pulmonary fluid imbalance ^{2, 23, 25, 26}. Pulmonary EC apoptosis
54 has been shown in experimental models of sepsis and ALI/ARDS ²⁷⁻³¹ and in ARDS clinical
55 samples ²¹. Despite these observations, and the possibility that improving lung EC survival could

56 be a useful strategy to combat ALI/ARDS^{32, 33}, the effect of differing severities of lung thrombosis
57 on pulmonary EC survival in ALI/ARDS is also unknown.

58 Given that anti-coagulants have failed in clinical trials of sepsis/ARDS³⁴⁻³⁷ and that
59 experimental thrombosis stimulates an angiogenic response^{38, 39}, we hypothesized that mild
60 levels of pulmonary thrombosis could protect against sepsis-induced ALI. In this study, we aimed
61 to determine the impact of varying levels of pulmonary thrombosis on sepsis-induced ALI, and to
62 delineate the underlying molecular mechanisms. We found that the induction of severe levels of
63 pulmonary thrombosis augmented EC apoptosis and ALI in sepsis mice, while a mild level of
64 pulmonary thrombosis conversely protected against ALI and mortality via endothelial
65 arachidonate 15-lipoxygenase (Alox15). EC-targeted overexpression of Alox15 inhibited the
66 increases in ALI caused by severe pulmonary thrombosis. Restoration of mild levels of pulmonary
67 thrombosis inhibited thrombocytopenia-induced increases in ALI and mortality in platelet-depleted
68 sepsis mice. The clinical relevance of the study was supported by our observation that there are
69 markedly reduced ALOX15-expressing ECs in the pulmonary vasculature of ARDS lungs
70 compared with normal lungs.

71

72 **Results**

73 ***Mild pulmonary thrombosis attenuates, whereas severe thrombosis augments,***
74 ***inflammatory lung injury in endotoxemia mice***

75 Pulmonary thrombosis may have protective or detrimental effects on ALI, so we first
76 investigated the impact of different levels of pulmonary thrombosis on ALI. Wild type (WT) mice
77 received various amounts of polystyrene microbeads (MBs) (i.v.) or vehicle to quantitatively
78 induce pulmonary thrombosis³⁹. At 24hrs later, mice received i.p. lipopolysaccharide (LPS) to
79 induce endotoxemia^{29, 40}, and lung injury was assessed at 36hrs post-LPS (i.e., at the time of
80 peak injury). A dose of 1,000 MBs/mouse led to the greatest reduction in lung vascular
81 permeability (as measured by Evans blue-conjugated albumin [EBA] flux) and neutrophil
82 sequestration (indicated by myeloperoxidase [MPO] activity)^{29, 40} versus MB-free endotoxic mice
83 (**Fig. 1, A and B**). Conversely, increasing the MB number resulted in dose-dependent increases
84 in lung vascular permeability, with 200,000 MBs/mouse resulting in highest levels of lung vascular
85 permeability versus vehicle-treated endotoxic controls (**Fig. 1A**). MPO activity was also markedly
86 increased in mice who received 200,000 MBs compared to MB-free endotoxic controls (**Fig. 1B**).
87 The protective dose of 1,000 MBs/mouse (referred to herein as innocuous) also reduced
88 apoptosis in pulmonary ECs compared with that found in MB-free endotoxic mice, while the
89 detrimental dose of 200,000 MBs/mouse (referred to herein as severe) worsened pulmonary EC
90 apoptosis (**Fig. 1, C to E**). In confirmatory studies, we verified that the innocuous MB dose did
91 indeed increase the levels of lung thrombosis above those found in vehicle-treated endotoxic
92 controls, and that this level was further enhanced by the severe dose of MBs (**Fig. 1, F to H**).

93 We next extended our studies of the protective effects of the innocuous level of pulmonary
94 thrombosis on lung injury. Consistent with reduced pulmonary vascular permeability (**Fig. 2A**),
95 1,000 MBs treatment decreased lung edema assessed by lung wet/dry weight ratio in sepsis-
96 challenged but not basal mice (**Fig. 2B**). Assessment of lung histology also revealed a marked

97 reduction in alveolar edema and septal thickening in 1,000 MBs-treated endotoxemic mice
98 compared to vehicle-treated endotoxemic mice (**Fig. 2, C to E**).

99 To determine whether the innocuous dose of MBs could inhibit inflammatory lung injury
100 when given after sepsis challenge, the 1,000 MBs were administered to WT mice at 2 or 8hrs
101 after LPS challenge. As shown in **Fig. 2, F and G**, the protective impact of this innocuous level of
102 pulmonary thrombosis on inflammatory lung injury, evidenced by marked reductions of lung EBA
103 flux and MPO activity at 36hrs post-LPS, was maintained even when the MBs were given at 8hrs
104 post-LPS challenge. Furthermore, treatment with 1,000 MBs promoted survival in mice
105 challenged with a lethal dose of LPS, regardless of whether the MBs were administered before
106 or after sepsis challenge (**Fig. 2H**). Together, these data demonstrate that while severe
107 pulmonary thrombosis enhance inflammatory lung injury, mild pulmonary thrombosis protects
108 against inflammatory lung injury induced by endotoxemia.

109

110 ***Molecular profiling of genes involved in the protective effects of mild lung thrombosis***

111 To elucidate molecular pathways through which mild pulmonary thrombosis protects
112 against inflammatory lung injury, we next performed RNA sequencing analysis. In these studies,
113 whole lung samples were analyzed from sepsis-free WT mice (basal group) and from LPS-treated
114 WT mice without MBs (vehicle group) or with mild (1,000 MBs/mouse) or severe (200,000
115 MBs/mouse) pulmonary thrombosis. Lung samples were collected for analysis at 24hrs post-LPS.
116 Of the 15,531 genes detected by RNA sequencing analysis, we selected the genes whose
117 expression levels varied from one group to another by ≥ 2 -fold, yielding a list of 82 genes. Of
118 these 82 genes, 12 are known to regulate cell survival (**Fig. 3A**). Of these 12 genes, the
119 expression patterns of 9 genes were validated in whole lung samples by qRT-PCR analysis (**Fig.**
120 **3B and Fig. S1**). The expression of 6 of these genes was increased in lung samples of LPS mice
121 treated with 1,000 MBs compared with mice receiving LPS alone, but not in LPS mice treated with

122 200,000 MBs (**Fig. 3B**). Quantitative (Q)RT-PCR analysis of isolated cells further showed that
123 these 6 genes were increased in either pulmonary non-ECs (i.e., Ghrl and Ms4a1), pulmonary
124 ECs (i.e., Alox15 and Cd22), or both pulmonary non-ECs and ECs (i.e., Pla2g2d and Serpinb2)
125 of 1,000 MBs-treated mice (**Fig. 3, C and D**). These data suggested that mild pulmonary
126 thrombosis could protect against inflammatory lung injury via attenuation of sepsis-induced
127 decreases of the expression of factors that regulate cell survival.

128

129 ***Endothelial Alox15 mediates the protective effects of mild lung thrombosis***

130 Given that mild lung thrombosis resulted in increased expression of Alox15 and Cd22 in
131 pulmonary ECs but not non-ECs, we next determined whether either of these factors was
132 responsible for the protective effects of mild thrombosis. We employed nanoparticle-targeted
133 delivery of an all-in-one CRISPR plasmid DNA expressing Cas9 under control of the human *CDH5*
134 promoter and guide RNA by the *U6* promoter, to delete either of these 2 genes selectively in ECs
135 of adult mice (**Fig. 4A**). Consistent with a previous study, which demonstrated ~80% decreases
136 in protein expression⁴¹, qPCR analysis demonstrated an approximately 40% genome editing
137 efficiency in the *Alox15* or *Cd22* locus in ECs but not non-ECs of the respective CRISPR plasmid-
138 transduced mice (**Fig. S2, A and B**). We confirmed an 80% decrease of EC-specific Alox15 at
139 the protein level (**Fig. 4B**). Seven days after nanoparticle:CRISPR plasmid DNA administration,
140 the mice receiving plasmid DNA expressing the scrambled guide RNA (WT group) or genome-
141 edited mice were administered either vehicle or 1,000 MBs followed by LPS challenge at 24hrs
142 after vehicle or MBs, and lungs were assessed at 36hrs post-LPS (**Fig. 4A**). As shown in **Fig. 4C**,
143 CRISPR-mediated disruption of endothelial *Alox15* but not *Cd22* reversed the 1,000 MBs-induced
144 decrease in pulmonary EBA flux. Consistently, lung MPO activity in endothelial *Alox15*- but not
145 *Cd22*-genome-edited mice treated with 1,000 MBs was markedly elevated compared to 1,000
146 MBs-treated WT mice (**Fig. 4D**). These data provide clear evidence that mild lung thrombosis

147 protects against inflammatory lung injury via endothelial Alox15 but not Cd22. Furthermore, we
148 observed endothelial-specific disruption of *Alox15* restored histological lung injury in 1,000 MBs-
149 treated mice to levels comparable with vehicle-treated WT mice, in contrast to 1,000 MBs-treated
150 WT mice (**Fig. 4, E and F**). Next, we showed that the inhibition of endothelial apoptosis by 1,000
151 MBs in WT mice was also reversed in *Alox15* genome-edited mice (**Fig. 4, G to I**). These data
152 together demonstrate that mild lung thrombosis reduces inflammatory lung injury via endothelial
153 Alox15.

154

155 ***Overexpression of Alox15 in ECs inhibits the detrimental effect of severe lung thrombosis*** 156 ***in septic mice***

157 Given that severe pulmonary thrombosis failed to reverse the sepsis-induced
158 downregulation of Alox15, we next determined whether restoration of expression of *Alox15* in ECs
159 could reverse the deleterious impact of severe lung thrombosis on ALI. Twenty hours after
160 administration of the mixture of nanoparticles:plasmid DNA expressing *Alox15* under the control
161 of *CDH5* promoter or empty vector, the mice were challenged with LPS, then treated with vehicle
162 or 200,000 MBs/mouse at 2hrs after LPS. Lungs were assessed at 36hrs post-LPS (**Fig. 5A**).
163 QRT-PCR analysis demonstrated a marked increase in *Alox15* mRNA expression selectively in
164 lung ECs of *Alox15* plasmid-transduced mice compared with vector mice (**Fig. S3**), which was
165 confirmed at the protein level (**Fig. 5B**). The 200,000 MBs-induced increase in pulmonary
166 vascular permeability was inhibited by EC-specific *Alox15* overexpression in *Alox15* plasmid-
167 transduced mice (**Fig. 5C**). Histological increases in lung edema and septal thickening caused by
168 200,000 MBs/mouse were also abolished by EC-specific *Alox15* overexpression in *Alox15*
169 plasmid-transduced mice with severe lung thrombosis (**Fig. 5, D and E**). Similarly, the severe lung
170 thrombosis-induced increase of lung EC apoptosis was also inhibited by EC-specific *Alox15*
171 overexpression (**Fig. 5, F to H**). These data suggest that increases in ALI resulting from severe

172 lung thrombosis can be reversed by an EC-targeted gene therapy approach to restore endothelial
173 Alox15 expression.

174

175 ***Restoration of mild levels of pulmonary thrombosis attenuate thrombocytopenic ALI***

176 Given that thrombocytopenia is associated with decreased survival in sepsis patients ^{12, 13}
177 and with increased risk of developing ARDS, as well as decreased survival in ARDS patients ¹⁴,
178 we next wished to determine whether thrombocytopenia-induced increases in ALI could be
179 inhibited through restoration of an innocuous level of lung thrombosis. To generate
180 thrombocytopenic mice, we used a genetic mouse model of platelet depletion in which
181 thrombocytopenia is induced by diphtheria toxin (DT) treatment of mice expressing the DT
182 receptor (DTR) in platelets and megakaryocytes controlled by *Pf4Cre* ⁴². We first showed that
183 circulating levels of platelets are reduced in this *DTR^{Pf4Cre}* model (i.e., PF4 group) to <10% of
184 levels found in *DTR^{Pf4-}* controls (i.e., WT group); this reduction occurred by day 2 after DT
185 treatment and remained suppressed to this extent for at least 3days (**Fig. S4A**) without altering
186 leukocyte numbers (**Fig. S4, B to G**). In subsequent studies of thrombocytopenic mice, LPS was
187 administered at the start of this period of platelet depletion and lungs were assessed at the time
188 point of peak injury (i.e., 36hrs post-LPS). While thrombocytopenia did not alter basal levels of
189 lung thrombosis in LPS-free mice, sepsis challenge gave rise to increases in lung thrombosis in
190 WT mice, and these increases were attenuated by thrombocytopenia (**Fig. S5. A to C**).
191 Concomitantly, in LPS-treated mice, thrombocytopenia resulted in exacerbated levels of
192 inflammatory lung injury, evidenced by increased lung EBA flux (**Fig. S6A**) and MPO activity (**Fig.**
193 **S6B**), as well as histological evidence of increased lung edema and alveolar septum thickening
194 (**Fig. S6, C to E**). These data demonstrate that thrombocytopenia impairs sepsis-induced lung
195 thrombosis and increases inflammatory lung injury.

196

197 To determine whether thrombocytopenia-induced increases in inflammatory lung injury
198 following sepsis challenge could be rescued by restoration of an innocuous level of lung
199 thrombosis, we next administered i.v. MBs at 24hrs prior to LPS challenge in thrombocytopenic
200 mice (**Fig. 6A**). Starting with the protective dose of 1,000 MBs/mouse identified above in WT mice,
201 we found that increasing doses of i.v. MBs gave rise to increasing levels of lung thrombosis in
202 thrombocytopenic sepsis-challenged mice, and that these increases occurred in a dose-
203 dependent manner (**Fig. 6, B and C**). The dose of MBs that restored lung thrombosis in PF4 mice
204 to the levels found in sepsis-challenged WT mice was 2,000 MBs/mouse (**Fig. 6, B and C**).
205 Importantly, 2,000 MBs/mouse did not alter the basal levels of lung EBA flux and MPO activity in
206 either platelet-replete (i.e., WT) or thrombocytopenic mice (data not shown). We then assessed
207 inflammatory lung injury in LPS-treated mice and found that this dose of 2,000 MBs/mouse
208 completely abolished the thrombocytopenia-induced increases in inflammatory lung injury as
209 assessed by histology (**Fig. 6, D to F**), EBA flux (**Fig. 6G**), and MPO activity (**Fig. 6H**). A dose of
210 2,000 MBs/mouse elicited the optimal protective effect compared to 1,000 MBs/mouse, 3,000
211 MBs/mouse, and 5,000 MBs/mouse (**Fig. 6, G and H**). However, a high dose of 100,000
212 MBs/mouse, resulting in excessive thrombosis (**Fig. 6C**), had no protective effects in PF4
213 thrombocytopenic mice and returned the levels of sepsis-induced inflammatory lung injury to that
214 found in MB-free thrombocytopenic mice (**Fig. 6, D to F**).

215 Next, we observed that the beneficial dose of 2,000 MBs/mouse inhibited
216 thrombocytopenia-induced increases in lung EBA flux and MPO activity, even when the MBs were
217 given at 2hrs after LPS (**Fig. 6, I and J**). Consistent with these findings, thrombocytopenia reduced
218 survival in PF4 mice challenged with lethal doses of LPS, but survival was improved by the
219 restoration of an innocuous level of lung thrombosis either before or after sepsis challenge (**Fig.**
220 **6K**). These data suggest that thrombocytopenia worsens ALI at least in part through impaired

221 lung thrombosis, and that restoration of an innocuous level of lung thrombosis can protect against
222 thrombocytopenia-induced ALI.

223

224 ***Mild pulmonary thrombosis is also protective against inflammatory lung injury induced by***
225 ***polymicrobial sepsis via endothelial Alox15***

226 We next determined the effects of various levels of pulmonary thrombosis on inflammatory
227 lung injury in a mouse model of polymicrobial sepsis induced by cecal ligation and puncture (CLP).
228 Similar to endotoxemia mice, sepsis-induced increases of EBA flux, MPO activity, endothelial
229 apoptosis, and histological lung injury were reduced in mice treated with 1,000 MBs/mouse
230 whereas exaggerated in mice treated with 200,000 MBs/mouse (**Fig. 7, A and B, Fig. S7, and**
231 **Fig. S8**). To determine if the protective effects of mild pulmonary thrombosis are also mediated
232 by endothelial Alox 15, we employed EC-targeted nanoparticle delivery of CRISPR/Cas9 plasmid
233 to selectively knockout *Alox15* in ECs in adult mice. The mice were then treated with 1,000
234 MBs/mouse followed by CLP challenge. As shown in **Fig. 7, C-I**, 1,000 MB-induced decreases in
235 EBA flux, MPO activity, endothelial apoptosis, and histological lung injury in WT mice were
236 abrogated in endothelial *Alox15* knockout mice.

237

238 ***ALOX15⁺ ECs are diminished in lung samples of ARDS patients***

239 To explore the clinical relevance of our findings, we assessed endothelial *ALOX15*
240 expression in human lungs. *In situ* RNA hybridization (RNAscope) assays of lung sections taken
241 postmortem from 6 ARDS patients (2 males, 4 females, 34-67 years old) and 6 unused normal
242 donor lungs (4 males, 2 females, 43-56 years old) revealed that the proportion of lung ECs that
243 were *ALOX15⁺* was markedly reduced in ARDS patients compared with normal controls (**Fig. 8,**
244 **A and B**). These data suggest that *ALOX15* in human lung ECs is also protective against
245 inflammatory lung injury.

246 Discussion

247 Our studies demonstrate that while a diminished or severely increased level of lung
248 thrombosis promotes sepsis-induced ALI, a mild level of lung thrombosis induces an EC survival
249 response and protects against ALI (**Fig. 8C**). Restoration of a mild level of lung thrombosis in
250 platelet-depleted mice inhibits the thrombocytopenia-induced increases in lung injury and
251 promotes survival. Furthermore, we show in 2 discrete mouse models of sepsis-induced ALI, that
252 the protective effects elicited by mild lung thrombosis are mediated by endothelial Alox15. Loss
253 of endothelial *Alox15* abolished the protective effects, while overexpression of endothelial *Alox15*
254 protected against severe thrombosis-induced increases in EC death and lung injury. In ARDS
255 patients, *ALOX15*⁺ ECs of the pulmonary vasculature were markedly reduced. Together, these
256 studies provide a comprehensive understanding of the role of varying levels of lung thrombosis in
257 the pathogenesis of inflammatory lung injury. Activation of ALOX15 signaling (e.g., via EC-
258 targeted nanoparticle delivery of the *ALOX15* gene) is a potential effective therapeutic strategy
259 for the treatment of ALI/ARDS caused by sepsis, particularly in patient sub-populations with
260 thrombocytopenia or severe pulmonary thrombosis.

261 In our studies, increasing doses of i.v. MBs were used to quantitatively induce lung
262 thrombosis in a stepwise manner. The MB size used in the current study (15 μ m diameter) was
263 selected to ensure seeding into the lung microvasculature³⁹. The same kind of MBs were also
264 used to induce lung thrombosis in a previous study of lung tumorigenesis in WT mice and
265 triggered a pro-angiogenic response in the pulmonary vasculature³⁹. We showed herein that the
266 innocuous level of lung thrombosis did not induce lung injury or inflammation in LPS-free (basal)
267 mice. It should be noted here that MBs have been previously used to induce chronic
268 thromboembolic pulmonary hypertension (CTEPH); the 15 μ m MBs used in our study, however,
269 are almost 6 times smaller than the MBs used to induce CTEPH in rats (85 μ m diameter)⁴³ and
270 20 times smaller than the MBs in dogs (100-300 μ m diameter)⁴⁴. Furthermore, in a previous rodent

271 study of CTEPH, a one-off dose of 388,000 MBs/rat (85µm diameter) failed to induce a
272 hypertensive response at 3 or 6wks after administration ⁴³, while repetitive administration of even
273 larger MBs (100-300µm diameter) every 3-4 days takes >100days and >25,000 MBs/animal to
274 induce a hypertensive response in dogs ⁴⁴. Although we did not assess pulmonary hypertension
275 in the current study, the one-off doses of 1,000 or 2,000 MBs/mouse did not cause any
276 discernable behavioral or respiratory changes or unexpected deaths in this study.

277 It has been suggested that severe levels of lung thrombosis could worsen ALI through
278 ischemia-induced cell death ¹⁸. Our study shows that a dose of 200,000 MBs/mouse does indeed
279 increase EC apoptosis and enhance ALI. Conversely, mild lung thrombosis induced by 1,000
280 MBs/mouse protected against ALI in septic WT mice. It has also been suggested that thrombosis
281 could protect against ALI by preventing bacterial transport between the lung and blood, by
282 providing a binding site for pro-survival factors and cytokines, and by blocking leaky endothelial
283 junctions ^{18, 45}. Here we show that mild lung thrombosis protects against lung EC apoptosis and
284 ALI and promotes mouse survival via endothelial Alox15. Alox15 is an enzyme producing 12- and
285 15-hydroxyeicosatetraenoic acid from arachidonic acid. In previous studies ⁴⁶⁻⁴⁸, allergen-induced
286 airway inflammation was diminished in global *Alox15* knockout mice, while global *Alox15*
287 deficiency increased inflammation and necroptosis in a murine dermatitis model, and *Alox15*-
288 overexpressing transgenic rabbits were protected against periodontitis. In experimental models
289 of murine ALI, global *Alox15* deletion or systemic inhibition has been previously shown to
290 decrease ALI following aerosolized LPS inhalation or intratracheal hydrochloric acid instillation,
291 which is largely mediated by hematopoietic Alox15, but global *Alox15* deletion instead increased
292 ALI following *A. fumigatus* infection. The apparent incongruence between reported findings could
293 be due to differences in experimental models and the use of global gene targeting methods, as
294 well as disparities resulting from pro- versus anti-inflammatory effects of Alox15 and its enzymatic
295 products ⁴⁹. Nevertheless, we found that *Alox15* expression in total lung and in lung ECs was

296 downregulated following LPS challenge and that the innocuous level of lung thrombosis could
297 attenuate sepsis downregulation of endothelial *Alox15* expression. Nanoparticle delivery of the
298 CRISPR system-mediated disruption of endothelial *Alox15* inhibited the protective effects of the
299 innocuous level of lung thrombosis and nanoparticle-targeted endothelial delivery of the *Alox15*
300 gene inhibited the severe thrombosis-induced increases in EC death and ALI in septic adult WT
301 mice. These EC-targeted gene therapy-like approaches avoided the potential confounding effects
302 of genetic compensation in transgenic/knockout mice as used in the aforementioned studies and
303 also modulate *Alox15* expression only in ECs. Our findings together provide strong support for a
304 pro-survival role of endothelial *Alox15* in lung ECs during inflammatory lung injury induced by
305 sepsis.

306 Finally, we employed a genetic mouse model of thrombocytopenia to show that platelet
307 depletion diminishes sepsis-induced lung thrombosis and increases inflammatory lung injury and
308 mortality in mice, and that the restoration of innocuous lung thrombosis protects against sepsis-
309 induced inflammatory lung injury in the setting of thrombocytopenia. The inducible genetic model
310 of thrombocytopenia enabled us to attenuate platelet levels and lung thrombosis without platelet-
311 depleting antibodies or anti-coagulants, which also influence inflammation. By combining genetic
312 thrombocytopenia with MB-induced lung thrombosis, we were able to diminish then restore lung
313 thrombosis in a quantitative and stepwise manner in platelet-depleted mice; this finding was not
314 entirely surprising, given that thrombi still form even when platelet numbers are reduced. It was
315 also unsurprising that a relatively higher dose of MBs (i.e., 2,000 MBs/mouse) was required to
316 induce the optimal protective level of lung thrombosis in thrombocytopenic compared with WT
317 mice (i.e., 1,000 MBs/mouse), given the established contribution of platelets to thrombus
318 formation. These studies help us understand the role of varying levels of thrombosis in the
319 pathogenesis of ALI and the failure of anti-coagulant therapies in clinical trials of sepsis/ARDS
320 patients³⁴⁻³⁷.

321 In summary, our studies provide unequivocal evidence that: (i) mild lung thrombosis
322 inhibits sepsis-induced ALI via endothelial Alox15; (ii) severe lung thrombosis increases sepsis-
323 induced ALI, which can be attenuated by EC overexpression of *Alox15*; (iii) normalization of lung
324 thrombosis inhibits thrombocytopenia-induced increases in ALI; and (iv) ARDS patients have
325 reduced levels of *ALOX15*⁺ lung ECs, which validates the clinical relevance of our findings. Our
326 surprising finding that mild lung thrombosis is protective may explain the lack of efficacy of anti-
327 coagulant therapies seen in clinical trials of sepsis/ARDS patients. Thus, tuning of lung
328 thrombosis to a protective level, or activation of ALOX15 signaling (e.g., through EC-targeted
329 nanoparticle delivery of endothelial ALOX15 gene), represent promising therapeutic strategies
330 against ALI/ARDS caused by sepsis.

331

332 **Materials and Methods**

333 **Mice.** Animal care and study protocols were reviewed and approved by the Northwestern
334 University Feinberg School of Medicine Institutional Animal Care and Use Committee. Male and
335 female C57BL/6J mice (aged 12-16wks) were used throughout the studies. For studies of
336 thrombocytopenia (i.e., platelet depletion), *Pf4Cre* mice (The Jackson Laboratories, USA) were
337 bred with *DTR* mice (The Jackson Laboratories, USA) to generate *DTR^{Pf4Cre}* mice (referred to
338 herein as PF4 mice). In these studies, littermate *Pf4Cre⁻* mice (*DTR^{Pf4⁻}*) served as WT controls
339 (referred to herein as WT mice). To induce genetic thrombocytopenia, *DTR^{Pf4Cre}* or *DTR^{Pf4⁻}* mice
340 received diphtheria toxin (DT) (20ng/g/day, i.p., Sigma-Aldrich, USA) for 3days. Blood was
341 collected by cardiac puncture into EDTA-coated tubes and complete blood cell counts were
342 performed using an automatic hematology analyzer (Advia 120, Siemens, USA).

343

344 **Nanoparticle-targeted EC-specific gene knockout and overexpression in adult mice.** EC-
345 specific disruption of *Alox15*, or *Cd22* expression in adult mice were achieved using nanoparticle-
346 mediated genome editing as described previously⁴¹. In short, EndoNP1 nanoparticles (Mountview
347 Therapeutics LLC, USA) were incubated at room temperature for 10mins with the all-in-one
348 plasmid DNA expressing Cas9 under the control of the EC-specific *CDH5* promoter and gene-
349 specific guide RNA driven by the *U6* promoter following the manufacturer's instructions, then
350 administered intravenously (retro-orbitally) to C57BL/6J WT adult mice (40µg plasmid
351 DNA/mouse). Seven days later, the genome-edited mice were used for studies. Mice treated with
352 nanoparticles plus plasmid DNA expressing scrambled RNA served as wild type (WT) controls.

353 EC-specific *Alox15* overexpression in adult mice was also achieved using nanoparticle-
354 mediated gene transduction. Briefly, EndoNP1 nanoparticles were mixed with plasmid DNA
355 expressing mouse *Alox15* driven by *CDH5* promoter or empty vector (control) for 10mins at room

356 temperature and then administered to C57BL/6J WT adult mice retro-orbitally (20µg of plasmid
357 DNA/mouse). Mice were sacrificed at 62hrs post-administration.

358

359 **Mouse model of endotoxemia.** To induce endotoxemia, mice received LPS (Santa Cruz
360 Biotechnology, Inc, USA) at a dose of 3mg/kg body weight for sub-lethal injury studies, and 4-
361 6mg/kg for survival studies, i.p. as previously described ^{29, 40}.

362

363 **Mouse model of polymicrobial sepsis.** To induce polymicrobial sepsis, mice underwent CLP
364 as previously described ⁴⁰. Briefly, mice were anesthetized with inhaled isoflurane (2.5% mixed
365 with room air). When the mouse failed to respond to paw pinch, buprenex (0.1 mg/kg) was
366 administered subcutaneously prior to proper sterilization of the skin with providone iodine, and
367 then a midline abdominal incision was made. The cecum was exposed and ligated with a 3-0
368 silk tie 1 cm from the tip and the cecal wall was perforated with a 20-gauge needle. Control
369 (sham) mice underwent anesthesia, laparotomy, and wound closure but no cecal ligation and
370 puncture. Immediately following the procedure, 500ul of warmed normal saline was
371 administered subcutaneously. Within 5min following surgery, the mice were able to wake from
372 anesthesia. The mice received a second dose of buprenex at 6-8h post-surgery
373 subcutaneously.

374

375 **Mouse model of pulmonary thrombosis.** To induce lung thrombosis, mice received polystyrene
376 microbeads (MBs, 15µm diameter, Invitrogen, USA) i.v. as previously described ³⁹.

377

378 **Lung histology.** Formalin-fixed paraffin-embedded lung sections (5µm) were stained with
379 hematoxylin and eosin (H&E) or martius scarlet blue (MSB) as previously described^{39,50}. Imaging
380 was performed using a brightfield microscope (Zeiss Axio, USA) with mounted camera and
381 integrated imaging software (ZEN 2.6, USA). Incidence of alveolar edema and septal thickening
382 were counted in a blinded manner in H&E-stained lung sections. Incidence of thrombosis and
383 fibrin area were assessed in a blinded manner in MSB-stained lung sections as previously
384 described^{39,50}. For each mouse, the incidence of edema, septal thickening, and microvascular
385 thrombosis was counted in 10 randomly selected 20x fields. Percentage fibrin coverage was also
386 assessed in 10 randomly selected 20x fields using image analysis software (ImageJ, NIH, USA).
387 Data are expressed as an average per field.

388

389 **Lung vascular permeability measurement.** Lung vascular permeability was assessed by
390 measurement of lung EBA flux as previously described⁴⁰. Briefly, EBA (20mg/kg) was injected
391 retro-orbitally 30mins before lungs were perfused with PBS free of blood. Lungs were then
392 collected, blotted dry, weighed, and homogenized in 0.5ml PBS and then incubated with 1ml
393 formamide at 60°C for 18hrs. Lung homogenates were centrifuged at 21,000g for 10mins. Optical
394 density of the supernatant was determined at 620nm and 740nm.

395

396 **Myeloperoxidase (MPO) activity assay.** Lung MPO activity was assessed as previously
397 described^{29,40}. Briefly, PBS-perfused lungs were homogenized in 0.5ml of 50mM phosphate
398 buffer. Homogenates were centrifuged at 21,000g for 15mins at 4°C. Thereafter, the pellets were
399 resuspended in phosphate buffer with 0.5% hexadecyl trimethylammonium bromide and
400 subjected to a freeze-thaw cycle. Subsequently, the homogenates were centrifuged at 21,000g
401 for 15mins at 4°C. Following addition of 34µl of sample to 10µl of O-dianisidine dihydrochloride

402 (16.7mg/ml) and 50µl of H₂O₂ (0.015% v/v) in 1ml of phosphate buffer, absorbance was measured
403 at 460nm every 20secs for 3mins.

404

405 **TUNEL staining.** Lung apoptosis was assessed by quantification of TUNEL-positive cells in lung
406 cryo-sections (5µm) using an In Situ Cell Death Detection Kit (Roche, USA) according to
407 manufacturer's instructions as previously described²⁹. Lung ECs were co-stained with anti-CD31
408 antibody (1:40 dilution, Abcam, USA) and anti-vWF antibody (1:250 dilution, Sigma, USA) for
409 18hrs at 4°C. Sections were incubated with Texas Red-conjugated secondary antibody (1:300
410 dilution, Invitrogen, USA) for 1hr at room temperature. Nuclei were counterstained with DAPI.
411 Imaging was performed using a confocal microscope (Zeiss LSM 880, USA) with mounted camera
412 and integrated imaging software (ZEN 2.6, USA). For each mouse, the number of apoptotic ECs
413 (CD31/vWF⁺ TUNEL⁺) and the number of apoptotic non-ECs (CD31/vWF⁻ TUNEL⁺) were counted
414 in a blinded manner in 10 randomly selected 25x fields. Data are expressed as an average
415 number per 1,000 nuclei.

416

417 **EC isolation.** CD31⁺ ECs and CD31⁻ non-EC fractions were isolated using magnetic-activated
418 cell sorting as previously described⁴⁰. Briefly, PBS-perfused lungs were cut into small pieces and
419 incubated in 1mg/mL collagenase A (Roche, USA) for 1hr at 37°C in a shaking water bath
420 (200rpm). The lung samples were then dissociated into a single-cell preparation using the
421 gentleMACS Dissociator (Miltenyi Biotec, USA) and filtered through a 40µm nylon cell strainer.
422 The single-cell preparation was then blocked with 20% fetal bovine serum for 30mins and
423 incubated with anti-CD31 antibody (Abcam, USA) for 30mins at room temperature, followed by
424 capture of CD31⁺ ECs with magnetic anti-rat IgG-conjugated Dynabeads (Invitrogen, USA) for

425 30mins. EC specificity was confirmed by quantitative RT-PCR (qRT-PCR) demonstration of EC
426 marker enrichment versus whole lung samples.

427

428 **RNA sequencing analysis.** RNA expression was assessed in whole lung tissues by RNA
429 sequencing analysis (Novogene, USA). Briefly, lung samples were collected after perfusion free
430 of blood and homogenized with Trizol (Invitrogen, USA) for RNA isolation. Isolated RNA was
431 further purified with RNeasy minikit (Qiagen, USA) with DNase I digestion to remove genomic
432 DNA. Purified RNA was sent to Novogene (USA) for RNA sequencing analysis.

433

434 **Molecular analyses.** To validate RNA sequencing data, RNA was isolated as described above.
435 Following reverse transcription, qPCR analysis was performed using the ABI ViiATM 7 real-time
436 PCR system (Thermo Fisher Scientific) with SYBR Green master mix to quantify the expression
437 of gene of interest. Mouse cyclophilin (*Cypa*) was used as housekeeping gene for normalization.
438 Nucleotide sequences are given in **Table S1**.

439 For quantification of genome editing efficiency, we employed a qPCR method as
440 described previously⁴¹. Isolated lung ECs and non-ECs were lysed in proteinase K solution
441 overnight at 60°C and genomic DNA was purified by standard pheno:chloroform extraction. qPCR
442 analysis of the wild-type genomic DNA without Indels was performed on genomic DNA samples
443 using the ABI ViiATM 7 real-time PCR system (Thermo Fisher Scientific) with SYBR Green master
444 mix. Nme1 genomic DNA amplification was used as normalization. Nucleotide sequences are
445 given in **Table S1**.

446 Protein levels of Alox15 were measured in isolated lung ECs and non-ECs by enzyme-
447 linked immunosorbent assay according to manufacturer's instructions (Abbeva, USA). Protein

448 levels are expressed per mg soluble protein as measured by the Bradford Assay according to
449 manufacturer's instructions (Bio-Rad, USA).

450

451 **Identification of potent guide RNA for *in vivo* study.** Potent guide RNAs were identified for *in*
452 *vivo* studies as previously described ⁴¹. Briefly, 4 guide RNAs for each gene were designed using
453 the Genscript guide RNA database and the correspondent DNA oligoes were subcloned to the
454 CRISPR^{CAG} plasmid DNA expressing antibiotic gene against puromycin. Hepa-1c1c7 cells
455 (ATCC, USA) were cultured in DMEM plus 10% FBS, 100U/ml penicillin, and 100µg/ml
456 streptomycin. At 50-70% cell density, the Hepa-1c1c7 cells in complete medium were transfected
457 with the all-in-one CRISPR^{CAG} plasmid DNA using EndoNP1 nanoparticles. The transfected cells
458 were then treated with puromycin (500ng/ml) for selection. The selected cells were then collected
459 for genomic DNA isolation by standard phenol:chloroform extraction. QPCR analysis was
460 performed on genomic DNA samples using the ABI ViiATM 7 real-time PCR system (Thermo
461 Fisher Scientific) with SYBR Green master mix. Nme1 genomic DNA amplification was used as
462 normalization. Nucleotide sequences are given in **Table S1**.

463

464 ***In situ* RNA hybridization (RNAscope analysis).** Formalin-fixed paraffin-embedded lung
465 sections from patients with ARDS or from normal control subjects (unused donor lungs) were
466 subjected to *in situ* RNA hybridization assay (RNAscope assay) for *ALOX15* mRNA expression
467 according to manufacturer's instructions (ACD Bio, USA). Lung ECs were co-immunostained with
468 anti-CD31 antibody (1:40 dilution, Abcam, USA) and anti-vWF antibody (1:250 dilution, Sigma,
469 USA) for 18hrs at 4°C. Sections were incubated with Texas Red-conjugated secondary antibody
470 (1:300 dilution, Invitrogen, USA) for 1hr at room temperature. Nuclei were counterstained with
471 DAPI. Imaging was performed using a confocal microscope (Zeiss LSM 880, USA) with mounted

472 camera and integrated imaging software (ZEN 2.6, USA). For each individual, the number of
473 ALOX15⁺ CD31/vWF⁺ ECs were counted in a blinded manner in 15 randomly selected blood
474 vessels. Data are expressed as an average percentage of blood vessel ECs.

475

476 **Human lung samples.** Archived post-mortem human lung samples from ARDS patients were
477 obtained from the University of Illinois at Chicago Biorepository. Lung samples from unused donor
478 lungs from the Pulmonary Hypertension Breakthrough Initiative (PHBI) were used as controls.
479 The use of these archived samples was approved by the Ann & Robert H. Lurie Children's
480 Hospital of Chicago Institutional Review Board.

481

482 **Statistical analysis.** Statistical analyses were performed using Prism 9 (Graphpad Software,
483 Inc., La Jolla, USA). Data normality was assessed using Shapiro-Wilk tests. Two group
484 comparisons were assessed with unpaired 2-tailed t-tests. Multiple group comparisons were
485 assessed using one- or two-way ANOVA with Bonferroni post-tests. Differences in survival were
486 assessed using the log-rank (Mantel-Cox) test. P values of <0.05 were considered significant.

487 **References**

- 488 1. Matthay MA, Zemans RL, Zimmerman GA, Arabi YM, Beitler JR, Mercat A, Herridge M,
489 Randolph AG, Calfee CS. Acute respiratory distress syndrome. *Nat Rev Dis Primers*.
490 2019;5:18
- 491 2. Lee WL, Slutsky AS. Sepsis and endothelial permeability. *N. Engl. J. Med.* 2010;363:689-
492 691
- 493 3. Rubenfeld GD, Caldwell E, Peabody E, Weaver J, Martin DP, Neff M, Stern EJ, Hudson
494 LD. Incidence and outcomes of acute lung injury. *N. Engl. J. Med.* 2005;353:1685-1693
- 495 4. Eichacker PQ, Parent C, Kalil A, Esposito C, Cui X, Banks SM, Gerstenberger EP, Fitz Y,
496 Danner RL, Natanson C. Risk and the efficacy of antiinflammatory agents: Retrospective
497 and confirmatory studies of sepsis. *Am J Respir Crit Care Med.* 2002;166:1197-1205
- 498 5. Opal SM, Fisher CJ, Jr., Dhainaut JF, Vincent JL, Brase R, Lowry SF, Sadoff JC, Slotman
499 GJ, Levy H, Balk RA, Shelly MP, Pribble JP, LaBrecque JF, Lookabaugh J, Donovan H,
500 Dubin H, Baughman R, Norman J, DeMaria E, Matzel K, Abraham E, Seneff M.
501 Confirmatory interleukin-1 receptor antagonist trial in severe sepsis: A phase iii,
502 randomized, double-blind, placebo-controlled, multicenter trial. The interleukin-1 receptor
503 antagonist sepsis investigator group. *Crit. Care Med.* 1997;25:1115-1124
- 504 6. Ware LB, Matthay MA. The acute respiratory distress syndrome. *N. Engl. J. Med.*
505 2000;342:1334-1349
- 506 7. Matthay MA, Ware LB, Zimmerman GA. The acute respiratory distress syndrome. *J. Clin.*
507 *Invest.* 2012;122:2731-2740
- 508 8. Ackermann M, Verleden SE, Kuehnel M, Haverich A, Welte T, Laenger F, Vanstapel A,
509 Werlein C, Stark H, Tzankov A, Li WW, Li VW, Mentzer SJ, Jonigk D. Pulmonary vascular
510 endothelialitis, thrombosis, and angiogenesis in covid-19. *N. Engl. J. Med.* 2020;383:120-
511 128

- 512 9. Matthay MA, Leligdowicz A, Liu KD. Biological mechanisms of covid-19 acute respiratory
513 distress syndrome. *Am J Respir Crit Care Med.* 2020;202:1489-1491
- 514 10. D'Agnillo F, Walters KA, Xiao Y, Sheng ZM, Scherler K, Park J, Gygli S, Rosas LA, Sadtler
515 K, Kalish H, Blatti CA, 3rd, Zhu R, Gatzke L, Bushell C, Memoli MJ, O'Day SJ, Fischer TD,
516 Hammond TC, Lee RC, Cash JC, Powers ME, O'Keefe GE, Butnor KJ, Rapkiewicz AV,
517 Travis WD, Layne SP, Kash JC, Taubenberger JK. Lung epithelial and endothelial
518 damage, loss of tissue repair, inhibition of fibrinolysis, and cellular senescence in fatal
519 covid-19. *Sci. Transl. Med.* 2021;13:eabj7790
- 520 11. Carsana L, Sonzogni A, Nasr A, Rossi RS, Pellegrinelli A, Zerbi P, Rech R, Colombo R,
521 Antinori S, Corbellino M, Galli M, Catena E, Tosoni A, Gianatti A, Nebuloni M. Pulmonary
522 post-mortem findings in a series of covid-19 cases from northern italy: A two-centre
523 descriptive study. *Lancet Infect. Dis.* 2020;20:1135-1140
- 524 12. Venkata C, Kashyap R, Farmer JC, Afessa B. Thrombocytopenia in adult patients with
525 sepsis: Incidence, risk factors, and its association with clinical outcome. *J Intensive Care.*
526 2013;1:9
- 527 13. Vandijck DM, Blot SI, De Waele JJ, Hoste EA, Vandewoude KH, Decruyenaere JM.
528 Thrombocytopenia and outcome in critically ill patients with bloodstream infection. *Heart*
529 *Lung.* 2010;39:21-26
- 530 14. Wang T, Liu Z, Wang Z, Duan M, Li G, Wang S, Li W, Zhu Z, Wei Y, Christiani DC, Li A,
531 Zhu X. Thrombocytopenia is associated with acute respiratory distress syndrome
532 mortality: An international study. *PLoS One.* 2014;9:e94124
- 533 15. ten Cate H, Schoenmakers SH, Franco R, Timmerman JJ, Groot AP, Spek CA, Reitsma
534 PH. Microvascular coagulopathy and disseminated intravascular coagulation. *Crit. Care*
535 *Med.* 2001;29:S95-97; discussion S97-98
- 536 16. Gando S, Levi M, Toh CH. Disseminated intravascular coagulation. *Nat Rev Dis Primers.*
537 2016;2:16037

- 538 17. Levi M, Ten Cate H. Disseminated intravascular coagulation. *N. Engl. J. Med.*
539 1999;341:586-592
- 540 18. Evans CE, Zhao YY. Impact of thrombosis on pulmonary endothelial injury and repair
541 following sepsis. *Am J Physiol Lung Cell Mol Physiol.* 2017;312:L441-L451
- 542 19. Levi M, Poll T. Coagulation in patients with severe sepsis. *Semin. Thromb. Hemost.*
543 2015;41:9-15
- 544 20. Semeraro N, Ammollo CT, Semeraro F, Colucci M. Sepsis, thrombosis and organ
545 dysfunction. *Thromb. Res.* 2012;129:290-295
- 546 21. Abadie Y, Bregeon F, Papazian L, Lange F, Chailley-Heu B, Thomas P, Duvaldestin P,
547 Adnot S, Maitre B, Delclaux C. Decreased vegf concentration in lung tissue and vascular
548 injury during ards. *Eur. Respir. J.* 2005;25:139-146
- 549 22. Bannerman DD, Goldblum SE. Mechanisms of bacterial lipopolysaccharide-induced
550 endothelial apoptosis. *Am J Physiol Lung Cell Mol Physiol.* 2003;284:L899-914
- 551 23. Aird WC. The role of the endothelium in severe sepsis and multiple organ dysfunction
552 syndrome. *Blood.* 2003;101:3765-3777
- 553 24. Evans CE, Iruela-Arispe ML, Zhao YY. Mechanisms of endothelial regeneration and
554 vascular repair and their application to regenerative medicine. *Am J Pathol.* 2021;191:52-
555 65
- 556 25. Maniatis NA, Kotanidou A, Catravas JD, Orfanos SE. Endothelial pathomechanisms in
557 acute lung injury. *Vascul. Pharmacol.* 2008;49:119-133
- 558 26. Millar FR, Summers C, Griffiths MJ, Toshner MR, Proudfoot AG. The pulmonary
559 endothelium in acute respiratory distress syndrome: Insights and therapeutic
560 opportunities. *Thorax.* 2016;71:462-473
- 561 27. Gill SE, Rohan M, Mehta S. Role of pulmonary microvascular endothelial cell apoptosis in
562 murine sepsis-induced lung injury in vivo. *Respir. Res.* 2015;16:109

- 563 28. Haimovitz-Friedman A, Cordon-Cardo C, Bayoumy S, Garzotto M, McLoughlin M, Gallily
564 R, Edwards CK, 3rd, Schuchman EH, Fuks Z, Kolesnick R. Lipopolysaccharide induces
565 disseminated endothelial apoptosis requiring ceramide generation. *J Exp Med.*
566 1997;186:1831-1841
- 567 29. Zhao YY, Gao XP, Zhao YD, Mirza MK, Frey RS, Kalinichenko VV, Wang IC, Costa RH,
568 Malik AB. Endothelial cell-restricted disruption of foxm1 impairs endothelial repair
569 following lps-induced vascular injury. *J. Clin. Invest.* 2006;116:2333-2343
- 570 30. Fujita M, Kuwano K, Kunitake R, Hagimoto N, Miyazaki H, Kaneko Y, Kawasaki M,
571 Maeyama T, Hara N. Endothelial cell apoptosis in lipopolysaccharide-induced lung injury
572 in mice. *Int Arch Allergy Immunol.* 1998;117:202-208
- 573 31. Wiener-Kronish JP, Albertine KH, Matthay MA. Differential responses of the endothelial
574 and epithelial barriers of the lung in sheep to escherichia coli endotoxin. *J. Clin. Invest.*
575 1991;88:864-875
- 576 32. de Souza PM, Lindsay MA. Apoptosis as a therapeutic target for the treatment of lung
577 disease. *Curr. Opin. Pharmacol.* 2005;5:232-237
- 578 33. Huertas A, Montani D, Savale L, Pichon J, Tu L, Parent F, Guignabert C, Humbert M.
579 Endothelial cell dysfunction: A major player in sars-cov-2 infection (covid-19)? *Eur. Respir.*
580 *J.* 2020;56
- 581 34. Ranieri VM, Thompson BT, Barie PS, Dhainaut JF, Douglas IS, Finfer S, Gardlund B,
582 Marshall JC, Rhodes A, Artigas A, Payen D, Tenhunen J, Al-Khalidi HR, Thompson V,
583 Janes J, Macias WL, Vangerow B, Williams MD, Group P-SS. Drotrecogin alfa (activated)
584 in adults with septic shock. *N. Engl. J. Med.* 2012;366:2055-2064
- 585 35. Vincent JL, Ramesh MK, Ernest D, LaRosa SP, Pacht J, Aikawa N, Hoste E, Levy H,
586 Hirman J, Levi M, Daga M, Kutsogiannis DJ, Crowther M, Bernard GR, Devriendt J,
587 Puigserver JV, Blanzaco DU, Esmon CT, Parrillo JE, Guzzi L, Henderson SJ, Pothirat C,
588 Mehta P, Fareed J, Talwar D, Tsuruta K, Gorelick KJ, Osawa Y, Kaul I. A randomized,

- 589 double-blind, placebo-controlled, phase 2b study to evaluate the safety and efficacy of
590 recombinant human soluble thrombomodulin, art-123, in patients with sepsis and
591 suspected disseminated intravascular coagulation. *Crit. Care Med.* 2013;41:2069-2079
- 592 36. Bernard GR, Ely EW, Wright TJ, Fraiz J, Stasek JE, Jr., Russell JA, Mayers I, Rosenfeld
593 BA, Morris PE, Yan SB, Helterbrand JD. Safety and dose relationship of recombinant
594 human activated protein c for coagulopathy in severe sepsis. *Crit. Care Med.*
595 2001;29:2051-2059
- 596 37. Dixon B, Smith RJ, Campbell DJ, Moran JL, Doig GS, Rechnitzer T, MacIsaac CM,
597 Simpson N, van Haren FMP, Ghosh AN, Gupta S, Broadfield EJC, Crozier TME, French
598 C, Santamaria JD. Nebulised heparin for patients with or at risk of acute respiratory
599 distress syndrome: A multicentre, randomised, double-blind, placebo-controlled phase 3
600 trial. *The Lancet. Respiratory medicine.* 2021;9:360-372
- 601 38. Evans CE, Humphries J, Mattock K, Waltham M, Wadoodi A, Saha P, Modarai B, Maxwell
602 PH, Smith A. Hypoxia and upregulation of hypoxia-inducible factor 1alpha stimulate
603 venous thrombus recanalization. *Arterioscler. Thromb. Vasc. Biol.* 2010;30:2443-2451
- 604 39. Evans CE, Palazon A, Sim J, Tyrakis PA, Prodger A, Lu X, Chan S, Bendahl PO, Belting
605 M, Von Euler L, Rundqvist H, Johnson RS, Branco C. Modelling pulmonary
606 microthrombosis coupled to metastasis: Distinct effects of thrombogenesis on
607 tumorigenesis. *Biology open.* 2017;6:688-697
- 608 40. Huang X, Dai Z, Cai L, Sun K, Cho J, Albertine KH, Malik AB, Schraufnagel DE, Zhao YY.
609 Endothelial p110gamma/pi3k mediates endothelial regeneration and vascular repair after
610 inflammatory vascular injury. *Circulation.* 2016;133:1093-1103
- 611 41. Zhang X, Jin H, Huang X, Chaurasiya B, Dong D, Shanley TP, Zhao YY. Robust genome
612 editing in adult vascular endothelium by nanoparticle delivery of crispr-cas9 plasmid DNA.
613 *Cell Rep.* 2022;38:110196

- 614 42. Wuescher LM, Takashima A, Worth RG. A novel conditional platelet depletion mouse
615 model reveals the importance of platelets in protection against staphylococcus aureus
616 bacteremia. *J. Thromb. Haemost.* 2015;13:303-313
- 617 43. Neto-Neves EM, Brown MB, Zaretskaia MV, Rezanian S, Goodwill AG, McCarthy BP,
618 Persohn SA, Territo PR, Kline JA. Chronic embolic pulmonary hypertension caused by
619 pulmonary embolism and vascular endothelial growth factor inhibition. *Am J Pathol.*
620 2017;187:700-712
- 621 44. Mulchrone A, Kellihan HB, Forouzan O, Hacker TA, Bates ML, Francois CJ, Chesler NC.
622 A large animal model of right ventricular failure due to chronic thromboembolic pulmonary
623 hypertension: A focus on function. *Front Cardiovasc Med.* 2018;5:189
- 624 45. Dixon B. The role of microvascular thrombosis in sepsis. *Anaesth. Intensive Care.*
625 2004;32:619-629
- 626 46. Andersson CK, Claesson HE, Rydell-Törmänen K, Swedmark S, Hällgren A, Erjefält JS.
627 Mice lacking 12/15-lipoxygenase have attenuated airway allergic inflammation and
628 remodeling. *Am J Respir Cell Mol Biol.* 2008;39:648-656
- 629 47. Serhan CN, Jain A, Marleau S, Clish C, Kantarci A, Behbehani B, Colgan SP, Stahl GL,
630 Merched A, Petasis NA, Chan L, Van Dyke TE. Reduced inflammation and tissue damage
631 in transgenic rabbits overexpressing 15-lipoxygenase and endogenous anti-inflammatory
632 lipid mediators. *J Immunol.* 2003;171:6856-6865
- 633 48. Zarbock A, Distasi MR, Smith E, Sanders JM, Kronke G, Harry BL, von Vietinghoff S,
634 Buscher K, Nadler JL, Ley K. Improved survival and reduced vascular permeability by
635 eliminating or blocking 12/15-lipoxygenase in mouse models of acute lung injury (ali). *J*
636 *Immunol.* 2009;183:4715-4722
- 637 49. Kühn H, Chan L. The role of 15-lipoxygenase in atherogenesis: Pro- and antiatherogenic
638 actions. *Curr. Opin. Lipidol.* 1997;8:111-117

639 50. Evans CE, Bendahl PO, Belting M, Branco C, Johnson RS. Diverse roles of cell-specific
640 hypoxia-inducible factor 1 in cancer-associated hypercoagulation. *Blood*. 2016;127:1355-
641 1360
642

643 **Acknowledgments**

644 We are grateful to the Biorepository at the University of Illinois at Chicago for the sections
645 of lung tissues from ARDS patients and to the Pulmonary Hypertension Breakthrough Initiatives
646 (PHBI) for the lung sections from unused donor lungs. This work was supported in part by NIH
647 grants R01HL123957, R01HL133951, R01HL148810, R01HL162299, and R01HL164014 to
648 Y.Y.Z and by an AHA Career Development Award 19CDA34500000 to C.E.E.

649

650 **Author Contributions**

651 C.E.E. and Y.Y.Z. conceived and designed the experiments. C.E.E., X.Z., and N.M.
652 performed the experiments. C.E.E., X.Z., and D.W. analyzed the data. C.E.E., D.W., and Y.Y.Z.
653 interpreted the data. C.E.E. wrote the manuscript. Y.Y.Z. supervised the project and revised the
654 manuscript.

655

656 **Competing Interests**

657 Y.Y. Zhao reported pending patent applications entitled “PLGA-PEG nanoparticles and
658 methods of uses”, “Cationic polymer-formulated nanoparticles and methods of use”. Y.Y. Zhao is
659 the founder and chief scientific officer of Mountview Therapeutics LLC. The authors have no
660 additional competing interests.

661

662 **Data and Materials availability**

663 All data are presented and included in the manuscript.

664 **Figures Legends**

665 **Fig. 1. Opposite effects of mild versus severe lung thrombosis on LPS-induced ALI. (A)**

666 Mice received either PBS vehicle (V) or indicated dose of MBs (i.v.) and 24hrs later received LPS
667 (3mg/kg, i.p.). Lung tissues were collected for analyses at 36hrs post-LPS. EBA flux assay was
668 used to demonstrate that a dose of 1,000 MBs/mouse protected against LPS-induced pulmonary
669 vascular permeability, but higher doses (e.g., 200,000 MBs/mouse) augmented LPS-induced
670 pulmonary vascular permeability. **(B)** MPO activity assay showing that 1,000 MBs/mouse
671 protected against whereas 200,000 MBs/mouse augmented LPS-induced lung neutrophil
672 sequestration. **(C-E)** TUNEL staining and quantification of apoptosis (green). ECs were stained
673 with anti-CD31 and anti-vWF antibodies (ECs, red). Nuclei were counterstained with DAPI (blue).
674 Arrows point to TUNEL⁺ ECs. Scale bar = 10 μ m. **(F-H)** MSB staining and quantification of thrombi
675 and fibrin area. Arrows indicate fibrin thrombi. Scale bar = 100 μ m. *P<0.05, **P<0.01, ***P<0.001,
676 and ****P<0.0001; one-way ANOVA with Bonferroni post-tests **(A-D, F, G)**.

677 **Fig. 2. Mild lung thrombosis protects against LPS-induced ALI and improves survival.** Mice
678 received PBS (Veh) or 1,000 MBs/mouse (i.v.) and 24hrs later received LPS (3mg/kg, i.p.) or PBS
679 (Basal). Lung tissues were collected for analyses at 36hrs post-LPS. **(A)** EBA flux assay showing
680 that treatment with 1,000 MBs/mouse reduced lung vascular permeability in LPS-treated but not
681 basal mice. Values for 36hrs post-LPS are repeated in Fig 1A and 2A. **(B)** The effect of 1,000
682 MBs/mouse on basal and LPS-induced lung edema was measured by lung wet/dry weight ratio.
683 Treatment with 1,000 MBs/mouse reduced lung edema in LPS-treated mice. **(C-E)** Histological
684 analysis of H&E-stained lung sections **(E)** showing that 1,000 MBs treatment reduced alveolar
685 edema **(C)**, and alveolar septum thickening **(D)** in LPS-treated mice compared to MB-free (Veh)
686 LPS-treated mice. In the representative images **(E)**, arrows point to alveolar edema and
687 arrowheads indicate thickened septum. Scale bar = 50 μ m. **(F, G)** The 1,000 MBs treatment given
688 after LPS challenge was also protective. At 2 or 8hrs after LPS (3mg/kg, i.p.), mice received PBS
689 (Veh) or 1,000 MBs (i.v.). At 36hrs post-LPS, lung tissues were collected for EBA flux assay **(F)**
690 and MPO activity measurement **(G)**. **(H)** Both pre- and post-LPS treatments with 1,000
691 MBs/mouse promoted survival. Mice received 1,000 MBs (i.v.) either 24hrs before (1k Pre-MBs)
692 or 2hrs after (1k Post-MBs) a lethal dose of LPS (6mg/kg, i.p.). Survival was monitored for 1wk.
693 n = 12/group. *P<0.05, **P<0.01, and ****P<0.0001; one-way **(F, G)** or two-way ANOVA **(A-D)**
694 with Bonferroni post-tests; log-rank (Mantel-Cox) test **(H)**.

695 **Fig. 3. The effects of lung thrombosis on expression of survival factors in lungs of sepsis-**
696 **challenged mice.** Mice received PBS (Veh) or indicated dose of MBs (i.v.) and 24hrs later were
697 challenged with LPS (3mg/kg, i.p.). At 24hrs post-LPS, lung tissues were collected for RNA
698 sequencing and qRT-PCR analyses. **(A)** Expression heatmap of survival genes that were
699 identified by RNA sequencing of whole lung samples to be downregulated in vehicle-treated LPS
700 mouse lungs versus basal mice and restored in LPS mice receiving 1,000 but not 200,000 MBs.
701 **(B)** QRT-PCR analysis confirming the effect of varying extents of lung thrombosis on the
702 expression patterns of survival genes in whole lungs of basal compared with sepsis-challenged
703 mice. **(C, D)** QRT-PCR analysis of expression of the survival factors in isolated pulmonary cells
704 from LPS-challenged mice, identifying gene induction by 1,000 MBs (MBs) in non-ECs (CD31⁻
705 cells) **(C)** and/or ECs (CD31⁺ cells) **(D)**. *Alox15* and *Cd22* were the 2 genes that were upregulated
706 only in ECs. *P<0.05, **P<0.01, and ****P<0.001; one-way ANOVA with Bonferroni post-test **(B)**
707 or independent t-tests **(C, D)**.

708 **Fig. 4. Mild lung thrombosis protects against LPS-induced ALI via endothelial Alox15. (A)**
709 Diagrammatical representation of the experimental procedure. Adult mice received a mixture of
710 nanoparticle:CRISPR^{CDH5} plasmid DNA expressing Cas9 under control of the human *CDH5*
711 promoter and gene-specific (*Alox15* or *Cd22*) guide RNA (designated as *Alox*^{ΔEC} or *Cd22*^{ΔEC},
712 respectively) or scrambled guide RNA (WT) driven by the *U6* promoter (40ug plasmid
713 DNA/mouse, i.v.). At 7days later, mice received PBS (Veh) or 1,000 MBs (i.v.) followed by LPS
714 challenge (3mg/kg, i.p.) at 24hrs later. Lung tissues were collected at 36hrs post-LPS for various
715 analyses. **(B)** ELISA analysis demonstrating diminished *Alox15* expression in lung ECs but not in
716 non-ECs isolated from CRISPR/*Alox15* gRNA-plasmid-administered basal mice. Lung tissues
717 were collected from mice at 7 days post-nanoparticle delivery of plasmid DNA. **(C)** CRISPR
718 plasmid DNA-mediated disruption of endothelial *Alox15* but not endothelial *Cd22* reversed the
719 decrease in pulmonary vascular permeability caused by treatment with 1,000 MBs/mouse. **(D)**
720 Knockdown of endothelial *Alox15* but not *Cd22* also reversed the 1,000 MBs treatment-elicited
721 decrease in MPO activity. **(E, F)** Quantitative analyses of H&E-stained lung sections showing
722 reversal of 1,000 MB treatment-induced decreases in alveolar edema **(E)**, and septum thickening
723 **(F)** in *Alox*^{ΔEC} mice. **(G-I)** Quantifications of pulmonary EC apoptosis **(G)** and total apoptosis **(H)**
724 in LPS-challenged mice. Lung cryosections were stained with FITC-TUNEL (apoptosis, green)
725 and anti-CD31/-vWF antibodies (ECs, red). Nuclei were counterstained with DAPI (blue). Arrows
726 point to TUNEL⁺ ECs **(I)**. Scale bar = 10μm. *P<0.05, **P<0.01, ***P<0.001, and ****P<0.0001;
727 two-way **(B)** or one-way ANOVA with Bonferroni post-tests **(C-H)**.

728 **Fig. 5. Overexpression of endothelial Alox15 inhibits the detrimental effects of severe lung**
729 **thrombosis on sepsis-induced lung injury. (A)** Diagrammatical representation of the
730 experimental procedure. **(B)** ELISA analysis demonstrating a marked increase of Alox15
731 expression in isolated lung ECs but not non-ECs of *Alox15* plasmid (*Alox15*)-transduced mice
732 compared to empty vector (V) mice. Human *CDH5* promoter was employed in the plasmid DNA.
733 **(C)** EBA flux assay demonstrating endothelial *Alox15* overexpression reversed the 200,000 MBs-
734 elicited increase of pulmonary vascular permeability in LPS mice. **(D, E)** Quantification of H&E-
735 stained mouse lung sections showing that overexpression of endothelial *Alox15* inhibited the
736 severe thrombosis-induced increases in alveolar edema **(D)** and septum thickening **(E)**. **(F-H)**
737 Quantifications of apoptosis in the lung demonstrating that 200,000 MBs/mouse-induced
738 increases in EC apoptosis **(F)** and total apoptosis **(G)** was inhibited by EC-specific *Alox15*
739 overexpression. Lung cryosections were stained with FITC-TUNEL (green) and with anti-CD31
740 and -vWF antibodies (ECs, red). Nuclei were counterstained with DAPI (blue). In the
741 representative micrographs **(F)**, arrows point to TUNEL⁺ ECs. Scale bar = 10µm. *P<0.05,
742 **P<0.01, and ****P<0.0001; one-way ANOVA with Bonferroni post-tests **(B-G)**.

743 **Fig. 6. Restoration of mild pulmonary thrombosis inhibits thrombocytopenia-enhanced**
744 **inflammatory lung injury in sepsis-challenged mice. (A)** Diagrammatical representation of the
745 experimental procedure. *DTR^{Pf4Cre}* (PF4) mice or *DTR^{Pf4-}* (WT) mice received DT (20ng/g/day,
746 i.p.) then PBS (Veh) or indicated dose of MBs (i.v.) followed by LPS (3mg/kg, i.p.). **(B)**
747 Representative images of MSB-stained lung cross-sections, showing apparent restoration of
748 thrombosis in thrombocytopenia PF4 mice by 2,000 MB treatment. Arrows indicate fibrin thrombi.
749 Scale bar = 100µm. **(C)** Quantifications of thrombi number revealing that thrombocytopenia
750 resulted in reduced pulmonary thrombosis in sepsis-challenged mice, which was reversible by
751 MB treatment. **(D)** Representative images of H&E lung cross-sections. Arrows indicate alveolar
752 edema. Arrowheads point to septal thickening. Scale bar = 50µm. **(E, F)** Quantifications of alveolar
753 edema and septal thickening. **(G)** EBA flux assay demonstrating that thrombocytopenia-induced
754 increase of pulmonary vascular permeability in PF4 mice was inhibited by treatment with low
755 doses (1,000-5,000) of MBs/mouse. **(H)** MPO activity assay. **(I)** Thrombocytopenia-induced
756 increase of pulmonary vascular permeability in PF4 LPS mice was reversed by post-sepsis
757 restoration of lung thrombosis. 2,000 MBs or PBS (Veh) were given at 2hrs after LPS. **(J)** MPO
758 activity. **(K)** Treatment with 2,000 MBs improved survival in thrombocytopenic LPS-challenged
759 mice. At 48hrs after final DT injection, mice received 4mg/kg LPS (i.p.). At 24hrs before (Pre-MBs)
760 or 2hrs after (Post-MBs) LPS challenge, mice received PBS (Veh) or 2,000 MBs. n = 8-9/group.
761 *P<0.05, **P<0.01, ***P<0.001, and ****P<0.001; one-way ANOVA with Bonferroni post-test **(C,**
762 **E-J)**; log-rank (Mantel-Cox) test **(K)**.

763 **Fig. 7. Mild lung thrombosis protects against CLP-induced ALI via endothelial Alox15. (A)**
764 Mice received either PBS vehicle (V) or indicated dose of MBs (i.v.) and 24hrs later received CLP.
765 Lung tissues were collected for analyses at 36hrs post-CLP. EBA flux assay was used to
766 demonstrate that a dose of 1,000 MBs/mouse protected against CLP-induced pulmonary vascular
767 permeability, but the high dose (i.e., 200,000 MBs/mouse) augmented CLP-induced pulmonary
768 vascular permeability. **(B)** MPO activity assay showing that 1,000 MBs/mouse protected against
769 whereas 200,000 MBs/mouse augmented CLP-induced lung neutrophil sequestration. **(C-I)** Adult
770 mice received a mixture of nanoparticle:CRISPR^{CDH5} plasmid DNA expressing Cas9 under control
771 of the human *CDH5* promoter and gene-specific (*Alox15*) guide RNA (designated as Δ EC) or
772 scrambled guide RNA (WT) driven by the *U6* promoter. At 7days later, mice received PBS vehicle
773 (V) or 1,000 MBs (i.v.) followed by CLP challenge at 24hrs later. Lung tissues were collected at
774 36hrs post-CLP for various analyses. CRISPR plasmid DNA-mediated disruption of endothelial
775 *Alox15* reversed the decrease in pulmonary vascular permeability caused by treatment with 1,000
776 MBs/mouse **(C)**. Knockdown of endothelial *Alox15* also reversed the 1,000 MBs treatment-elicited
777 decrease in MPO activity **(D)**. TUNEL staining and quantification of apoptosis (green) **(E, F)**. ECs
778 were stained with anti-CD31 and anti-vWF antibodies (ECs, red). Nuclei were counterstained with
779 DAPI (blue). Arrows point to TUNEL⁺ ECs. Scale bar = 10 μ m. Quantitative analyses of H&E-
780 stained lung sections showing reversal of 1,000 MB treatment-induced decreases in alveolar
781 edema **(G)** and septum thickening **(H)** in *Alox1^{EC}* mice. In the representative images **(I)**, arrows
782 point to alveolar edema and arrowheads indicate thickened septum. Scale bar = 50 μ m. *P<0.05,
783 **P<0.01, ***P<0.001, and ****P<0.0001; one-way ANOVA with Bonferroni post-tests **(A-D, F, G)**.

784 **Fig. 8. ALOX15⁺ ECs were markedly reduced in lungs of non-survival ARDS patients. (A)**
785 Representative images of *in situ* RNA hybridization (RNAscope) assays for *ALOX15* expression
786 (green) in archived postmortem lung paraffin sections from ARDS patients and unused donor
787 controls. ECs were immunostained with anti-CD31 and -vWF antibodies (red). Nuclei were
788 counterstained with DAPI (blue). Arrows indicate *ALOX15⁺* lung ECs. Scale bar = 10 μ m. **(B)**
789 Quantification of *ALOX15⁺* ECs in lung sections showing reduced *ALOX15⁺* ECs in lung sections
790 from ARDS patients compared with normal controls. *P<0.05; unpaired t-test. **(C)** Diagrammatical
791 summary of key findings. Mild lung thrombosis reduces sepsis-induced inflammatory lung injury,
792 whereas severe or impaired lung thrombosis induced by thrombocytopenia augments sepsis-
793 induced inflammatory lung injury. Restoration of lung thrombosis in platelet-depleted mice inhibits
794 the thrombocytopenia-induced increase in lung injury and promotes survival. The protective
795 effects elicited by mild lung thrombosis are mediated by inhibiting the sepsis-induced
796 downregulation of endothelial Alox15, which promotes EC survival.

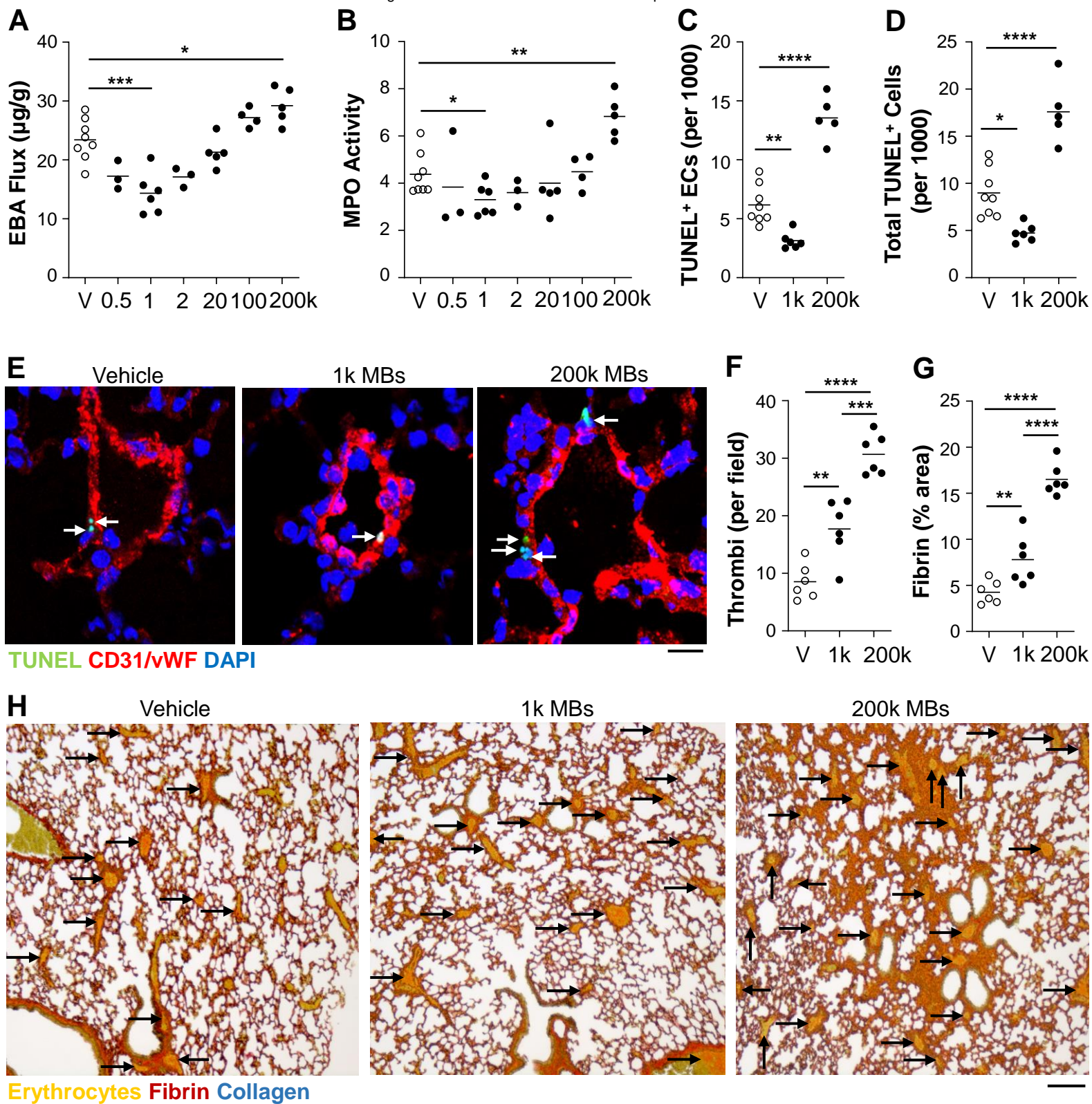


Figure 1

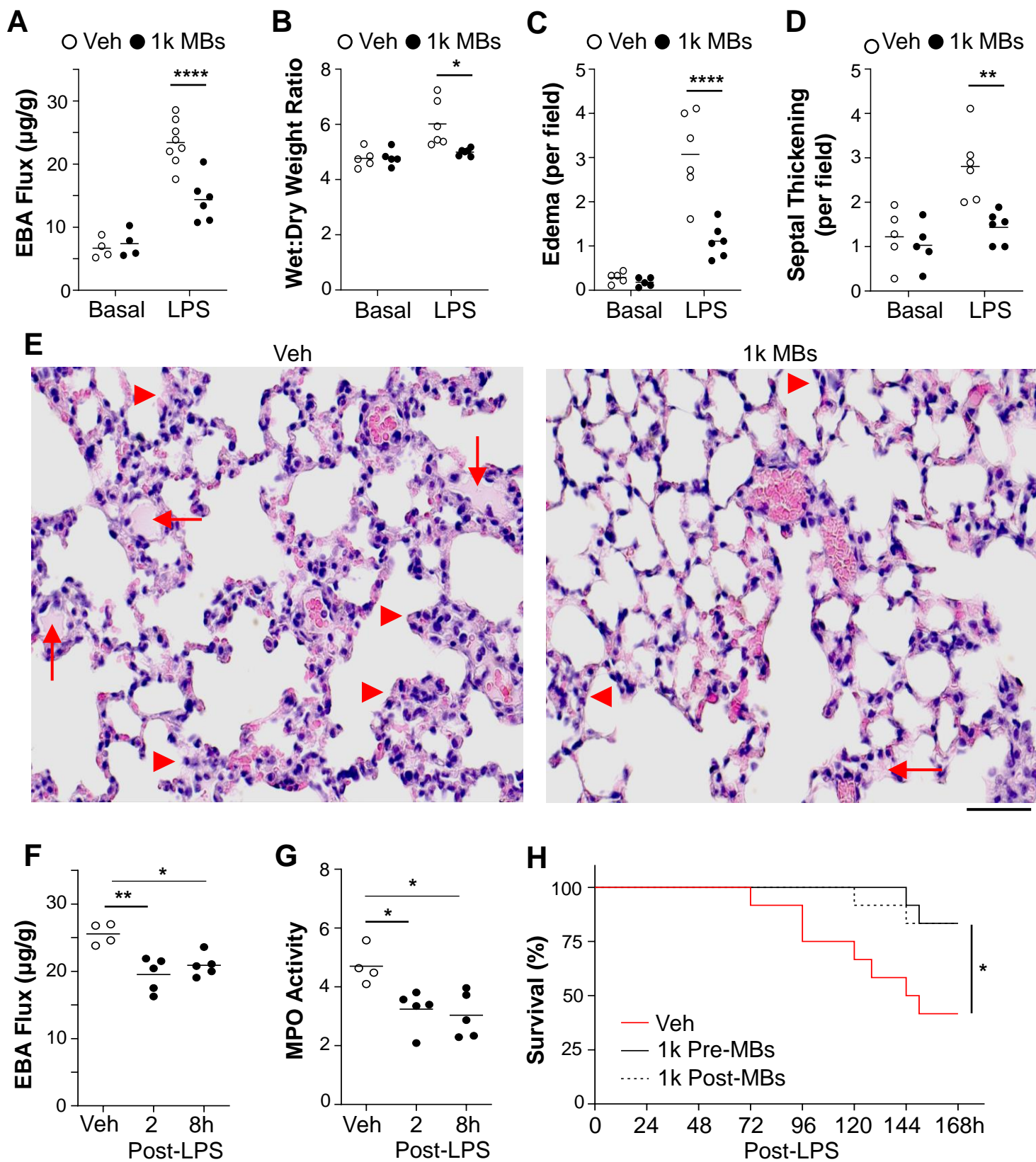
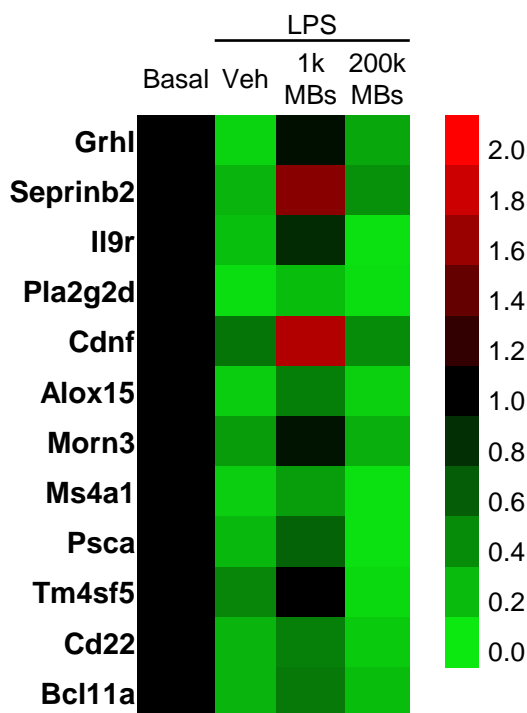
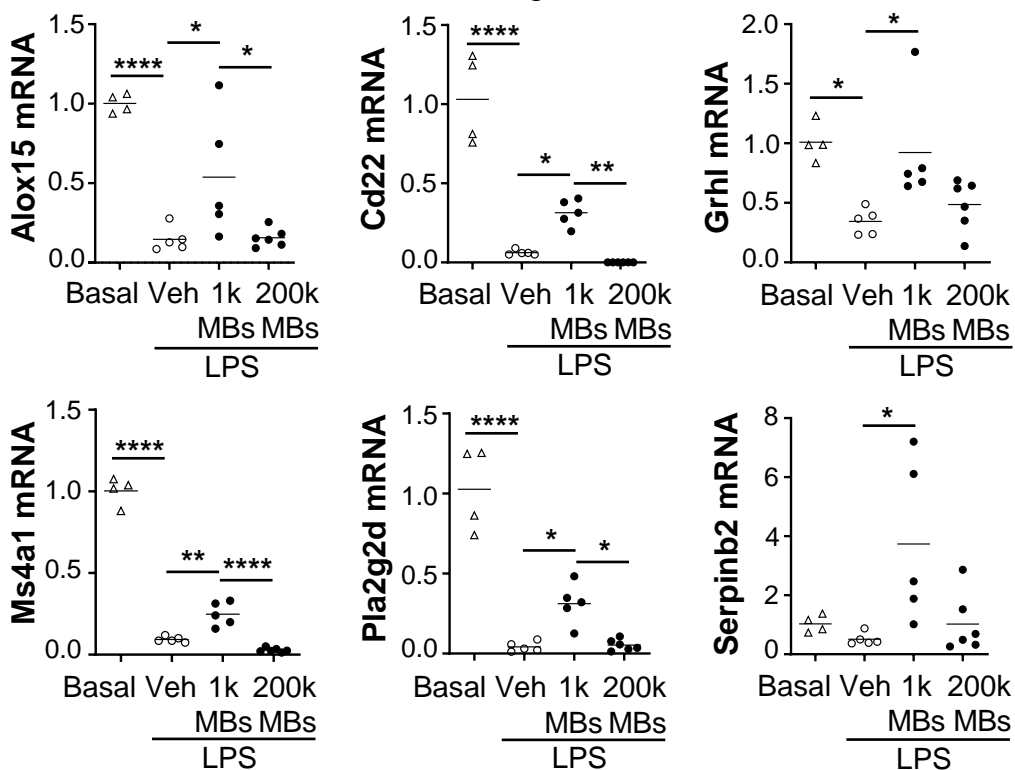


Figure 2

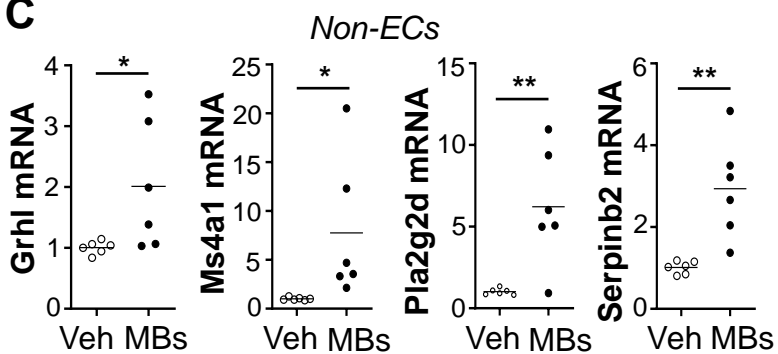
A



B



C



D

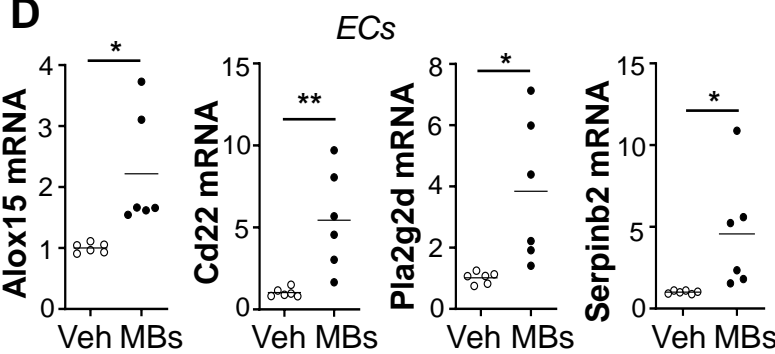


Figure 3

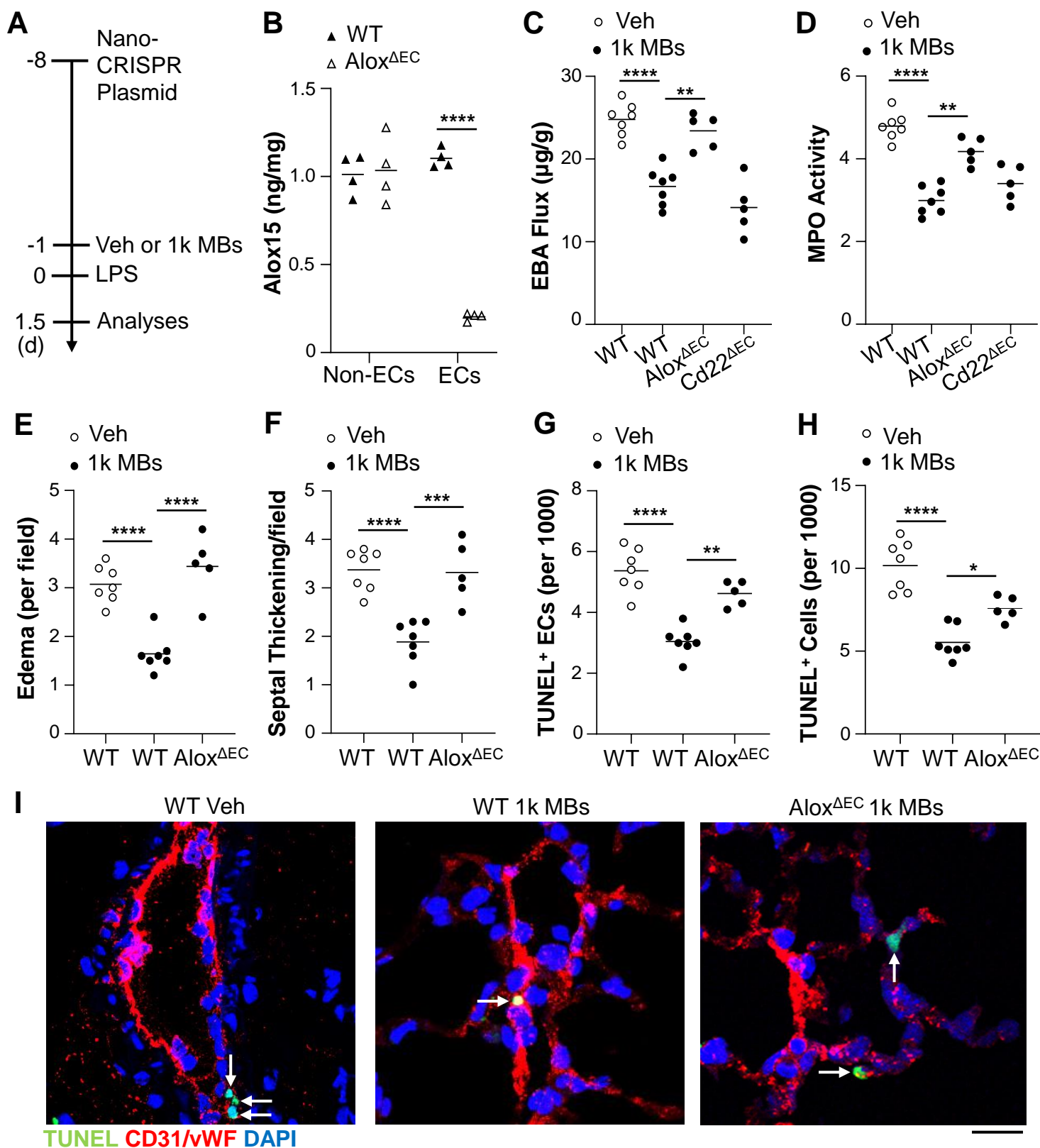


Figure 4

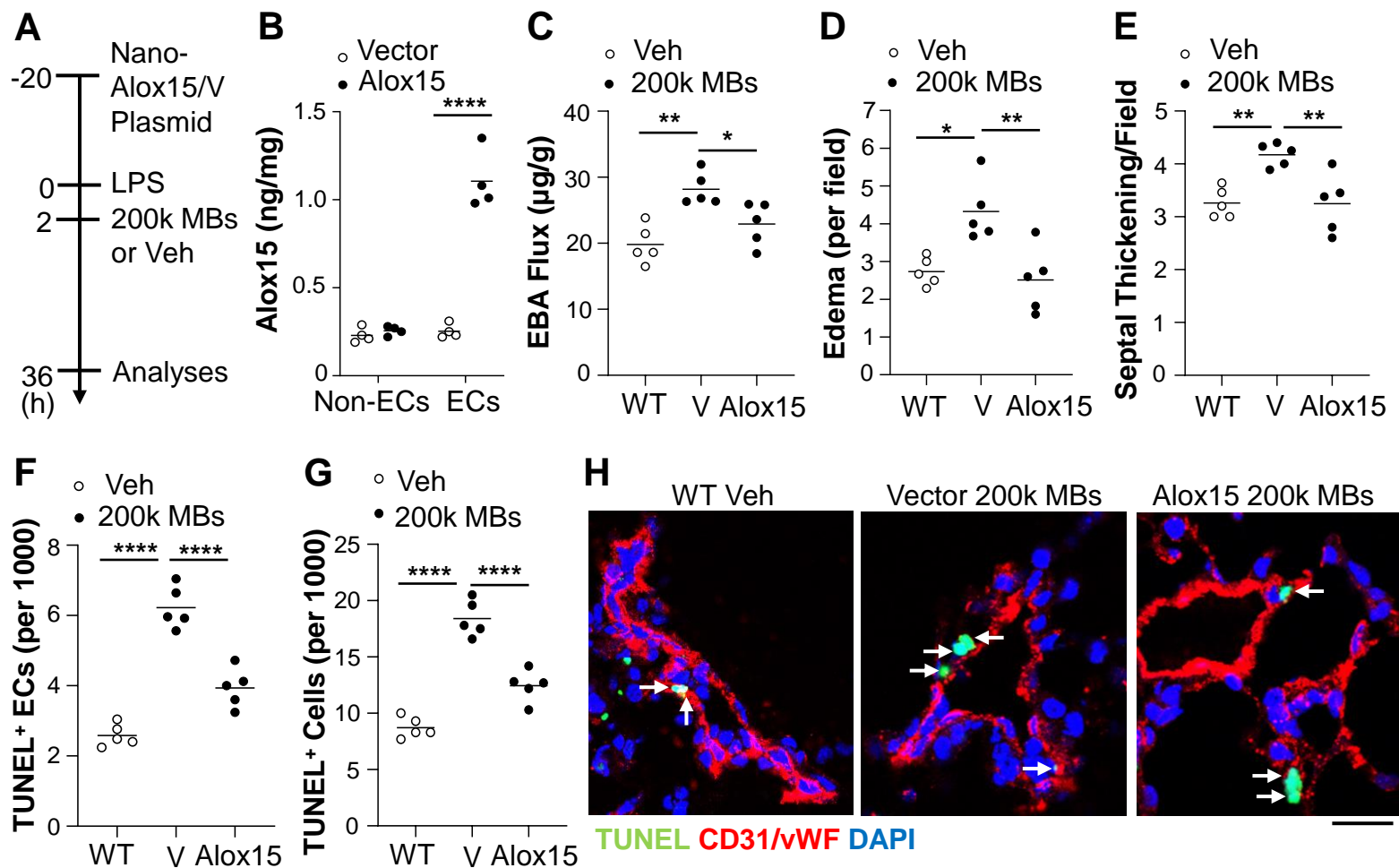


Figure 5

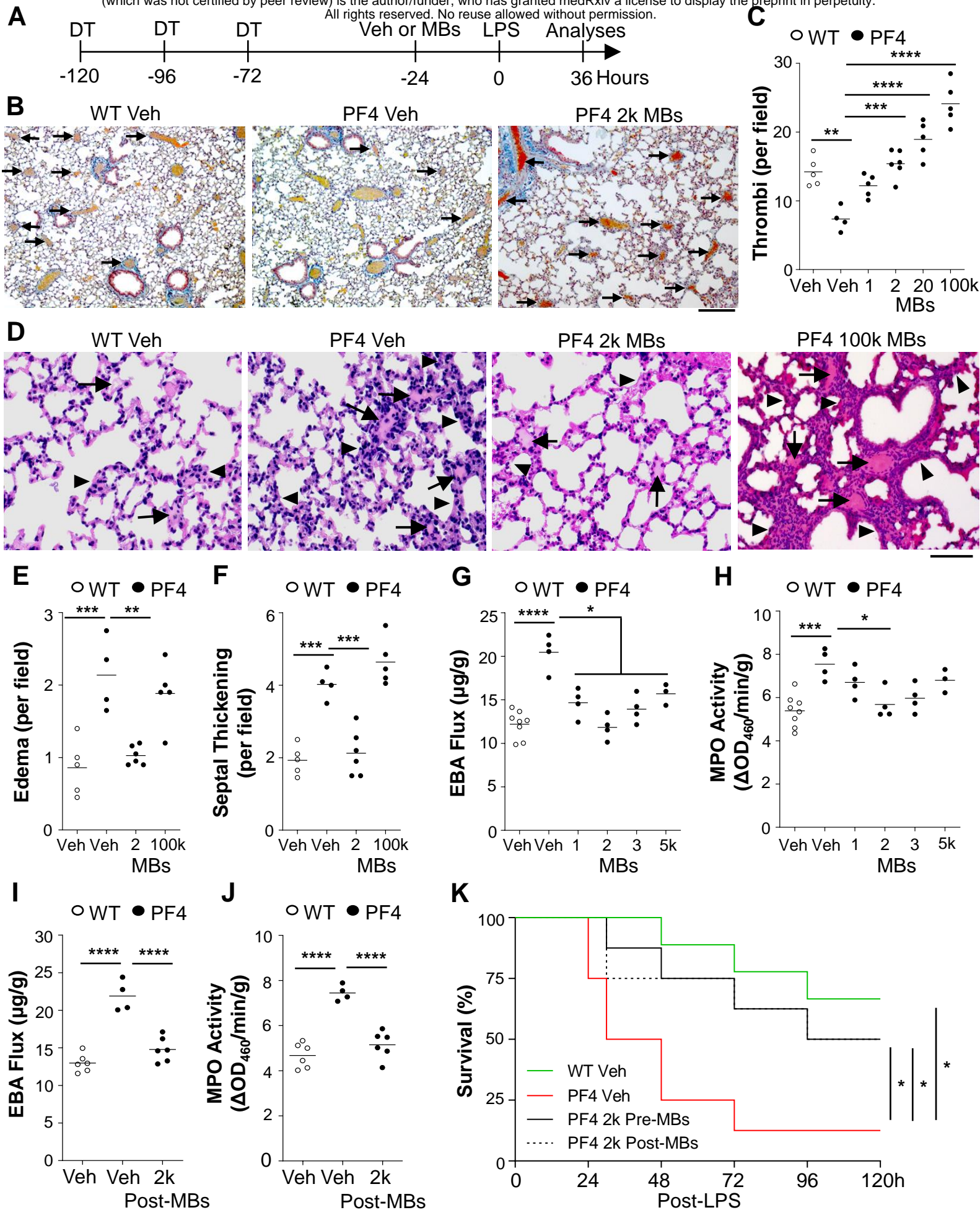


Figure 6

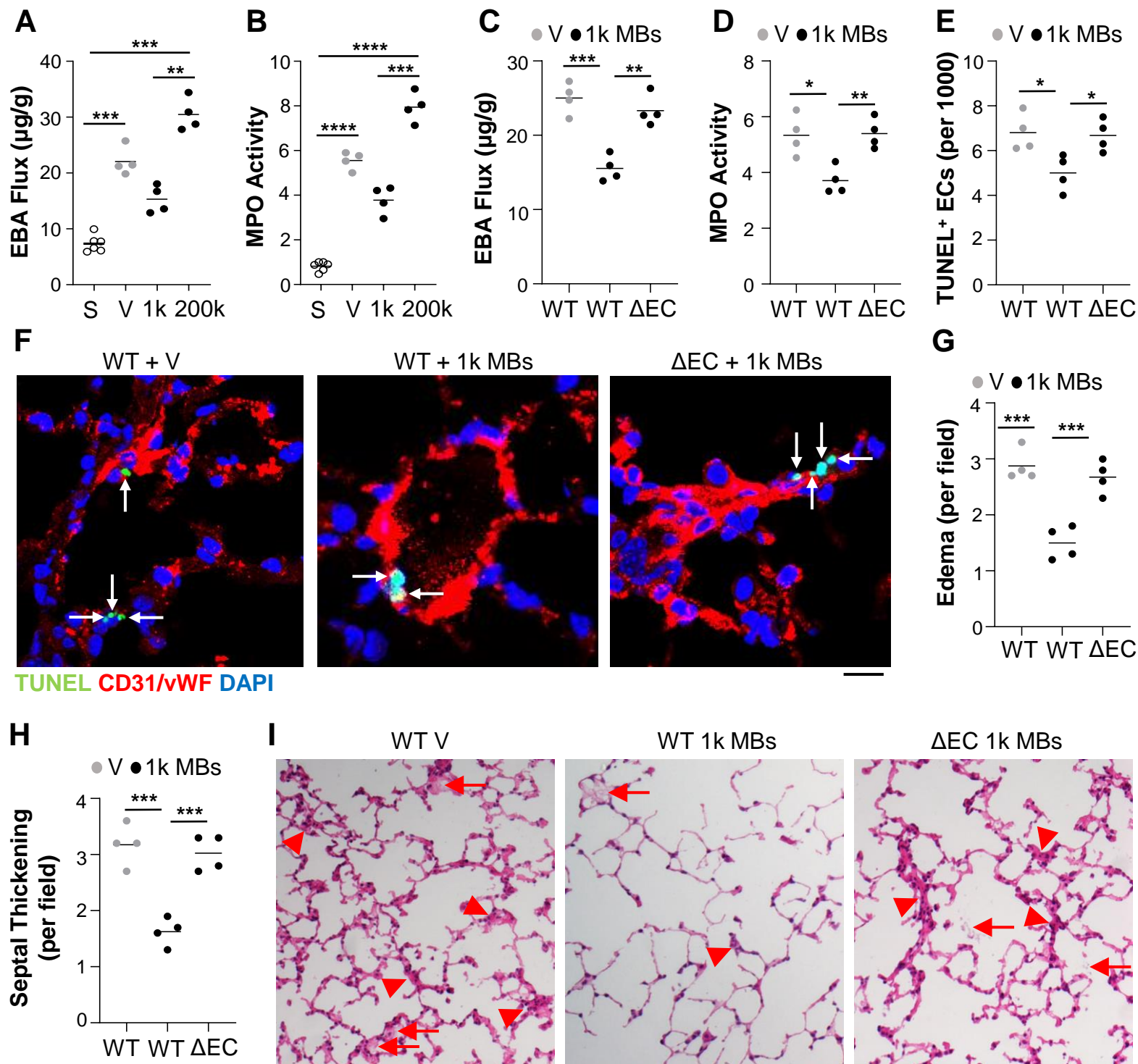


Figure 7

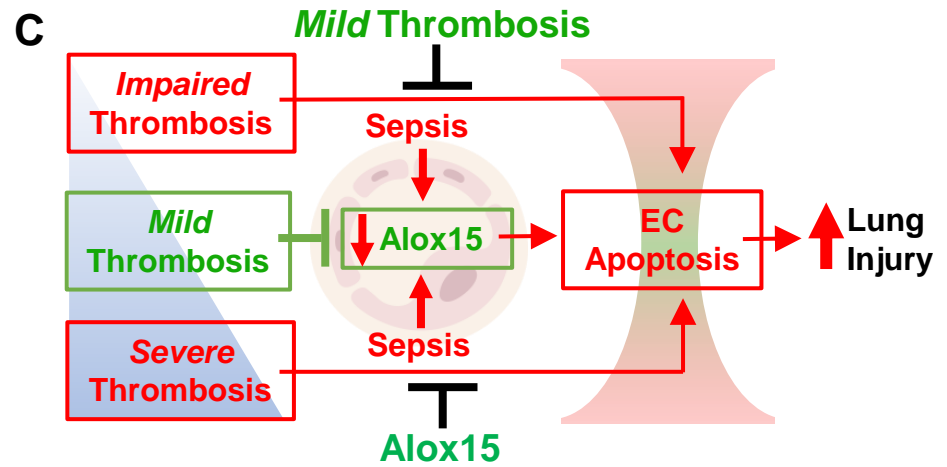
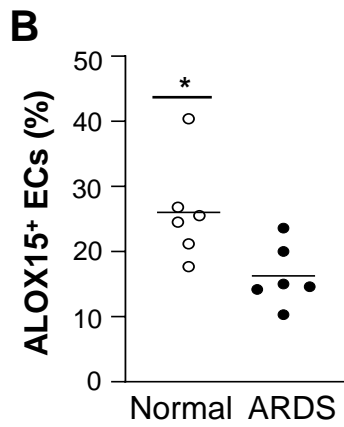
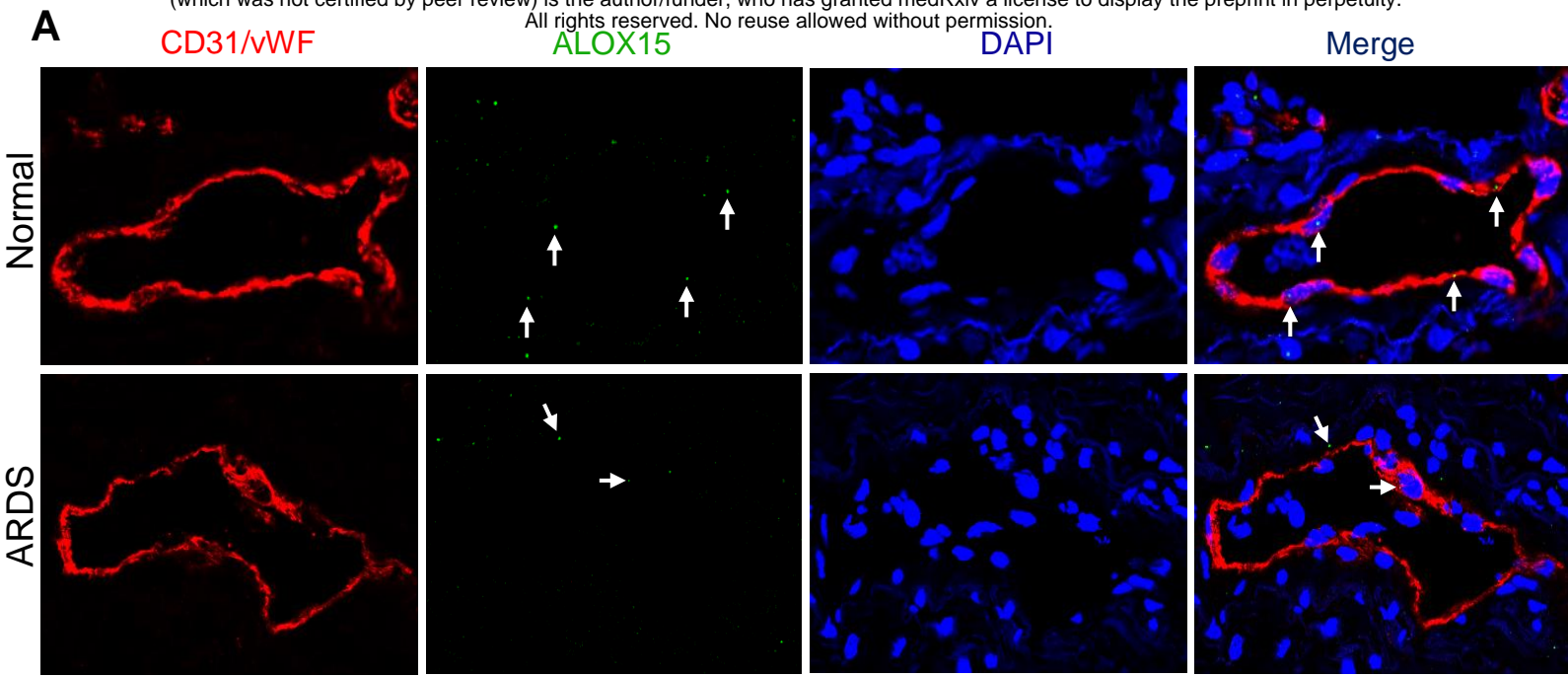


Figure 8